MOLECULAR HYBRID CONTAINING ANTICANCER DRUG AND RECOGNIZING COLORECTAL CANCER CELLS

BY

KANPITCHA JIRAMITMONGKON

A DISSERTATION SUBMITTED IN PARTIAL FULFILLMENT OF THE REQUIREMENTS FOR THE DEGREE OF DOCTOR OF PHILOSOPHY (CHEMISTRY)

DEPARTMENT OF CHEMISTRY

FACULTY OF SCIENCE AND TECHNOLOGY

THAMMASAT UNIVERSITY

ACADEMIC YEAR 2025

MOLECULAR HYBRID CONTAINING ANTICANCER DRUG AND RECOGNIZING COLORECTAL CANCER CELLS

BY

KANPITCHA JIRAMITMONGKON

A DISSERTATION SUBMITTED IN PARTIAL FULFILLMENT OF THE REQUIREMENTS FOR THE DEGREE OF DOCTOR OF PHILOSOPHY (CHEMISTRY)

DEPARTMENT OF CHEMISTRY

FACULTY OF SCIENCE AND TECHNOLOGY

THAMMASAT UNIVERSITY

ACADEMIC YEAR 2025

THAMMASAT UNIVERSITY

FACULTY OF SCIENCE AND TECHNOLOGY

DISSERTATION

BY

KANPITCHA JIRAMITMONGKON

ENTITLED

MOLECULAR HYBRID CONTAINING ANTICANCER DRUG AND RECOGNIZING COLORECTAL CANCER CELLS

was approved as partial fulfillment of the requirements for the degree of Doctor of Philosophy (Chemistry)

on , 2025

Chairman _____
(Associate Professor Apiwat Chompoosor, Ph.D.)

Member and Advisor _____
(Associate Professor Boonchoy Soontornworajit, Ph.D.)

Member and Co-adviser _____
(Paisan Khanchaitit, Ph.D.)

Member _____
(Associate Professor Panumart Thongyoo, Ph.D.)

Member _____
(Assistant Professor Jiraporn Arunpanichlert, Ph.D.)

Dean _____
(Associate Professor Supet Jirakajohnkool, Ph.D.)

Dissertation Title	MOLECULAR HYBRID CONTAINING ANTICANCER DRUG AND RECOGNIZING COLORECTAL CANCER CELLS
Author	Kanpitcha Jiramitmongkon
Degree	Doctor of philosophy (chemistry)
Department/Faculty/University	Chemistry Faculty of Science and Technology Thammasat University
Dissertation Advisor	Associate Professor Boonchoy Soontornworajit, Ph.D.
Dissertation Co-Advisor	Paisan Khanchaitit, Ph.D.
Academic Year	2025

ABSTRACT

Colorectal cancer (CRC) constitutes a major public health burden both in Thailand and globally, necessitating the development of more effective treatments. Nevertheless, current therapeutic strategies remain constrained by limited specificity and efficacy. To overcome these challenges, a multifunctional drug delivery platform was developed by incorporating bioactive materials with specific recognition ligands into a unified molecular construct. Aptamers could function as specific binding ligands for cancer treatment formulation. They are short single-stranded synthetic chemical DNA or RNA sequences. These agents possess the ability to bind target molecules with high affinity and specificity. Therefore, the aptamers were used as recognition agents in the drug delivery systems. In addition, antisense oligonucleotides (ASOs) interrupt transcription processes resulting in specifically inhibiting or silencing target mRNA pathways. This research aimed to construct a multifunctional drug delivery system that contains AS1411 aptamer, T9/U4 ASO, and doxorubicin for regulating C cell proliferation. Due to the specific affinity of AS1411 aptamer for nucleolin, a protein abundantly expressed on the cell membrane of various cancers. T9/U4 ASO suppressed cancer cell proliferation by inhibiting human telomerase RNA activity. Research activities for this project are as follows: i) AS-T9/U4 molecular hybrid (AS-T9/U4_MH) was prepared by oligonucleotide hybridization ii) aptamer train (AT) was

formed through hybridization and ligation reaction. The anti-cancer drugs doxorubicin (Dox) and mitoxantrone (MTZ) were loaded into AS-T9/U4_MH and AT, respectively. Evaluation of the effects of anti-cancer drug–loaded molecular hybrids on cell proliferation was performed using the MTS assay. Subsequently, the molecular hybrid capable of binding was assessed via flow cytometry and fluorescence microscopy. The results showed that AS-T9/U4_MH and AT specifically recognize C cells because they have nucleolin on their surface. Moreover, AS-T9/U4_MH and AT showed antiproliferation. Dox and MTZ loaded systems showed that Dox and MTZ were encapsulated resulting in less toxicity. These results suggest that the multifunctional drug delivery system is a promising system for incorporating other chemotherapeutic drugs to other bioactive materials and the delivery system would be used for cancer treatment.

Keywords: doxorubicin, antisense oligonucleotides, AS1411 aptamer, nucleolin, hybridization, colorectal cancer

ACKNOWLEDGEMENTS

I would like to express my deepest gratitude to my supervisor, Associate. Professor Boonchoy Soontornworajit, Ph.D., and Paisan Khanchaitit, Ph.D., for their invaluable guidance, insightful feedback, and unwavering encouragement throughout the course of this research. Their expertise and patience have greatly contributed to the completion of this thesis.

I am also sincerely thankful to the members of my thesis committee, Associate Professor Apiwat Chompoosor, Ph.D., Associate Professor Panumart Thongyoo, Ph.D., and Assistant Professor Jiraporn Arunpanichlert, Ph.D., for their valuable comments and suggestions, which significantly enhanced the quality of this work.

My appreciation extends to my colleagues and fellow researchers in the Aptamer Research Group, whose technical assistance, stimulating discussions, and collaborative spirit made this journey both productive and enjoyable.

I would like to thank the Thammasat Funding Research Unit, Full Scholarship for Research, Internationalization, and Education, Thammasat University, for the Academic Year 2025, and National Science and Technology Development Agency for their financial support, without which this research would not have been possible.

On a personal note, I'm grateful to my family and friends for their unwavering love, patience, and support during this difficult time. Their steadfast belief in me was my greatest motivation.

Finally, I dedicated this thesis to Aptamer Research Group as a token of my gratitude for their inspiration and unwavering faith in my abilities.

Kanpitcha Jiramitmongkon

TABLE OF CONTENTS

LIST OF TABLES

LIST OF FIGURES

LIST OF NOMENCLATURE

Symbols/Abbreviations	Name
A cell	CCD841 CoN cell
B cell	Caco-2 cell
C cell	SW480 cell

LIST OF ABBREVIATIONS

Symbols/Abbreviations	Terms
%	Percent
/	Per
<	Less than
=	Equal
>	More than
μg	Microgram
μl	Microliter
μM	Micromolar
ASOs	Antisense oligonucleotides
AT	Aptamer train
ATP	Adenosine 5′-triphosphate
BCA	Bicinchoninic acid
CRC	Colorectal cancer
CT	Control train
DAPI	4′,6′-diamidino-2-phenylidoledihydrochloride
DMEM	Dulbecco's modified eagle medium
Dox	Doxorubicin
DTT	Dithiothreitol
FAM	Carboxyfluorescein
FBS	Fetal bovine serum
FITC	Fluorescein isothiocyanate
HBS	Hybridization strand
MH	Molecular hybrid
$MgCl_2$	Magnesium chloride
MTZ	Mitoxantrone
PBS	Phosphate buffer saline

PI	Propidium Iodide
PVDF	Polyvinylidene fluoride
SD	Standard deviation
SDS-PAGE	Sodium dodecyl sulfate-Polyacrylamide gel electrophoresis
SELEX	Systematic Evolution of Ligands by Exponential Enrichment
TBS	Tris-Buffer Saline
TEMED	*N,N,N′,*N′- Tetramethylethylenediamine
Tris-HCl	Tris(hydroxymethyl)aminomethane hydrochloride

CHAPTER 1
INTRODUCTION

1.1 Rational background

Cancer is the second leading cause of human mortality worldwide due to limitations on early diagnosis and high-precision treatment. The annual number of new cancer diagnoses and cancer-related deaths continues to increase. In 2021, the National Cancer Institute reported that the first common cancer found in Thai people both men and women was colorectal cancer (CRC). Chemotherapy is one of practical and reliable strategy for cancer treatment and it is used in the combination with other strategies including surgical resection, and radiotherapy [1]. However, the chemotherapy prone to have limitations in poor selectivity for cancer cells, resulting in adverse effects on normal cells and leading to treatment failure and patient suffering [2]. For example, a major drawback of doxorubicin (Dox), a common anticancer drug, is its cardiotoxicity [3]. Lefrak et.al demonstrated that dose of Dox over 600 mg/m^2 induced cardiomyopathy increasing up to 36% [4]. Swain et.al. observed that when the patients received Dox to the maximum does of 550 mg/m^2, they suffered a congestive heart failure up to 26% [5]. Challenges on cancer treatment that have been faced include recurrence and drug resistance and they require more understandings about cellular activities. Many biological processes such as cell proliferation, morphogenesis, and blood vessel formation play key role on cancer progression and they are controlled by various signaling pathways. In general, the aberrant signaling pathways cause normal cells to develop themselves into cancer cells [6, 7]. Moreover, cancer cells also use these aberrant mechanisms to develop metastasis. Therefore, the development of safe and effective treatment strategies necessitates minimizing side effects, reducing the risk of recurrence, and preventing the emergence of drug resistance. Although targeted therapy, immunotherapy, and gene therapy show promising results in laboratory studies, they are less effective in clinical study. This inspires the quest for alternative treatments by incorporating the key drugs relying on the nanotechnology findings. The findings yield reliable delivery vehicles that exhibit specific targeting, and enhanced

cellular uptake property [8-10]. The use of binding ligands—such as short peptide, aptamers, and small molecules—can give a substance the ability to target specific cells or tissues [11-13].

Aptamer-mediated nano-vehicles are promising drug delivery systems for anticancer. Their strong binding ability and effective treatment characteristics make them suitable for a wide range of applications. Aptamers are small nucleic acid segments that have the function of inhibiting and binding to target species and they are applied for targeted therapies [14]. AS1411 aptamer is able to bind to nucleolin that is overexpressed in various cancer cells such as lung cancer, CRC, and breast cancer [15]. Aptamers act as a recognition element, targeting a biomarker on the outer surface of a tumor cell. Additionally, the aptamers work as a cargo for carrying cytotoxic agents (eg. anticancer drugs) and eventually bring the drugs into the cells [16-19].

To further enhance an effectiveness of treatment, an addition of another active ingredient that yields synergistic effect is a good strategy. It was reported that antisense oligonucleotides (ASOs) exhibited anticancer property and was facile to be incorporated with the aptamers via hybridization [20]. ASOs are small molecules targeting a specific mRNA or pre-mRNA sequences. They work by using Watson-Crick base pairing to hybridize with their complementary RNA sequence, which can lead to various effects. They inhibited functions of RNA by mediating the cleavage of the mRNA-DNA duplex and blocking a specific protein translation [21]. The ASO named T9/U4 inhibited telomerase activity by complementary binding to a telomerase template region. Consequently, the tumor cells stopped proliferating [22]. In this proposed work, the T9/U4 ASO was a promising choice for integrating with AS1411 aptamer and anticancer drug via oligonucleotide hybridization yielding a multifunctional drug delivery system that could differentiate between cancer cells and normal cells. This could minimize toxic side effects.

1.2 Research problem

In this study, we hypothesized that the multifunctional drug delivery system specifically targeted a certain biomarker on CRC and effectively regulated the cell proliferation. Therefore, how to prepare of molecular hybrid composed of AS1411

aptamer, T9/U4 ASO, and anti-cancer drug (Dox and MTZ) were investigated. Effect of this molecular hybrid on CRC activities was characterized to address the merits of this therapeutic system.

1.3 Objective

The objective of this work is to develop multifunctional drug delivery systems which recognize colorectal cancer cells. Research tasks are proposed as follows.

1) To prepare a molecular hybrid composed of AS1411 aptamer and T9/U4 ASO assigned as AS – T9/U4_MH via oligonucleotide hybridization (**Fig 1.1**).

2) To prepare an aptamer molecular train (AT) composed of AS1411 aptamer using hybridization coupled with enzymatic ligation (**Fig 1.2**).

3) To incorporate Dox into AS – T9/U4_MH and MTZ into AT by using intercalation strategy.

4) To test binding capability of AS – T9/U4_MH and AT on A, B and C cells by fluorescence microscope and flow cytometer.

5) To study the effects of the two molecular hybrids on cancer cells proliferation and related cellular pathways.

1.4 Outcome

1) This study will provide us feasible ways for preparing the multifunctional molecular hybrids between recognition elements and bioactive compounds.

2) Understandings of the functions of these molecular hybrids in an *in vitro* experiment could initiate further studies on animal models and clinical trials.

3) The success of those studies will enable us to use the molecular hybrids as effective chemotherapeutic agents.

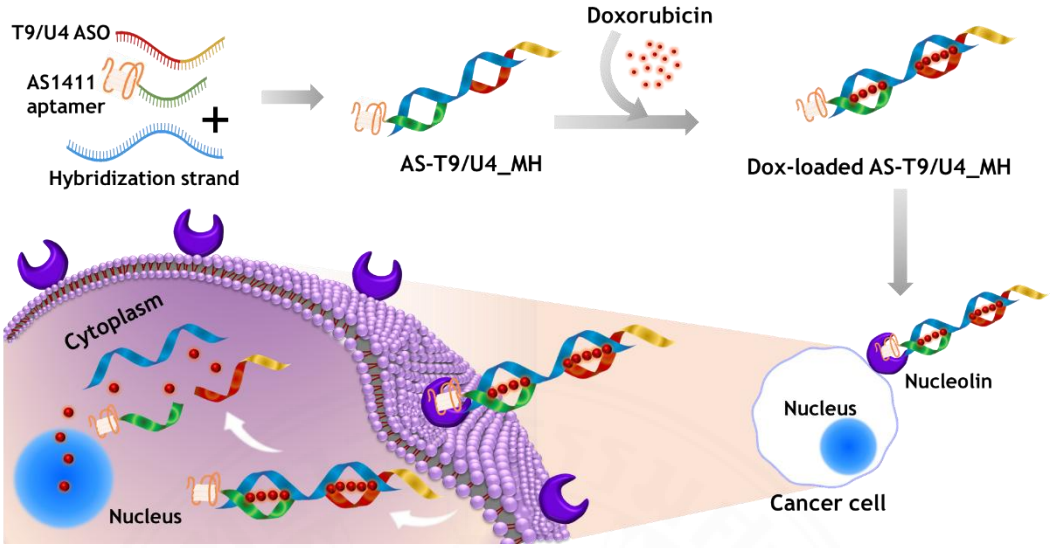

Fig 1.1 The concept of AS-T9/U4_MH preparation.

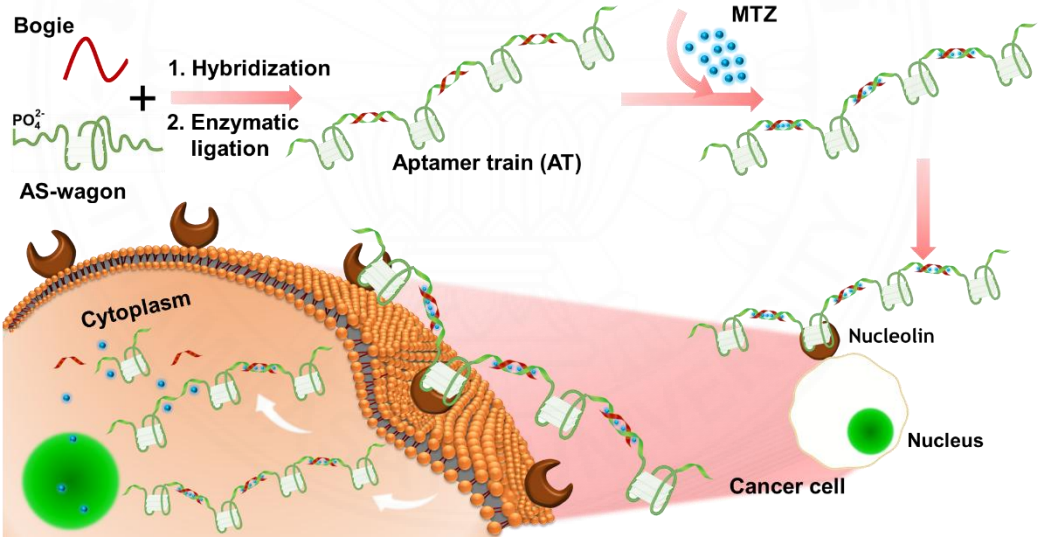

Fig 1.2 The concept of aptamer train (AT) preparation.

CHAPTER 2
REVIEW OF LITERATURE

2.1 Nanotechnology in medicine

Advances in nanotechnology are enabling the development of new nanomaterials that have a wide range of applications in biology, chemistry, and medicine. DNA and RNA, which carry genetic information in living organisms serve as building blocks for nanomaterials. DNA nanostructures that carry controllability and versatility function have drawn interest to the field [23]. A number of DNA nanostructures have been developed ranging from simple to complicated structures such as DNA simple tiles, [24] cubes, [25] tetrahedrons, [26, 27] octahedrons, [28, 29] and DNA dendrimers [30, 31]. Compared to other nanomaterials, DNA nanostructures are highly versatile as following aspects. The use of hydrogen bonding to form nucleobase pairs (A-T/U and G-C) makes it possible to create predictable and programmable nucleic acid nanostructures [23]. The conformation and orientation of DNA nanostructures are predictable resulting in many structures that are suitable for each application [32]. The various external stimuli affecting the nanostructures such as temperature, [33] pH, [34] and ionic strength [35] are used to tune functionality of the DNA nanostructures. In addition, the alteration of DNA sequences and lengths is a practical strategy for modifying DNA nanostructure properties. The DNA nanostructures exhibited no detectable toxicity toward normal cells in both *in vivo* and *in vitro* assays [26]. Finally, there are a number of DNA nanostructures forming by the Watson-Crick base pairing such as aptamer, [36] siRNA, [37] and ASO, [21] that exhibit biological functions. Aptamers are small nucleic acid segments that have the function of inhibiting and binding to target species (eg. small molecules, proteins, and cells). Silencing RNA is a non-coding RNA sequence made of two strands, which is designed to silence gene expression. It is usually between 21 – 23 oligonucleotides in length which is capable of binding to the target mRNA and inducing consequently gene silencing at the post-transcription process. Gene silencing triggers the degradation of messenger RNA (mRNA), thereby inhibiting the subsequent translation of protein. An ASO is a short, engineered DNA strand that works by recognizing and binding to a

specific site on a target mRNA. This binding, which relies on Watson-Crick base pairing, causes the mRNA to be degraded. From these candidates, aptamers are molecules of our interest because they carry recognition ability and have been extensively studied for developing the DNA nanostructure. These advantages of DNA nanostructure could be benefit to medical diagnosis and therapeutic applications.

2.2 Aptamer

2.2.1 Aptamer overview

Aptamers, first identified by Andrew Ellington in 1990, are short single-stranded DNA (ssDNA) or RNA molecules capable of folding into unique secondary and three-dimensional structures. By adopting these specific conformations, aptamers can recognize and bind to targets such as small molecules, proteins, or whole cells with remarkable specificity and affinity, functioning in a manner similar to antibodies but with advantages such as smaller size and lower immunogenicity [38, 39]. Due to their characteristics, aptamers are considered excellent candidates to replace antibodies.

Normally, aptamers are isolated from a diverse library of random sequences using a method known as Systematic Evolution of Ligands by Exponential Enrichment (SELEX). This process helps identify the sequences that bind most effectively to a specific target [40-43]. The procedures start with the chemical synthesis of DNA molecules, which is a random library containing 10^{14}-10^{16} different oligonucleotides. SELEX cycle consists of iterative binding, separating, eluting, and amplifying **(Fig. 2.1).** At the end SELEX cycle, the pool is enriched with ligands capable of binding target molecules with high specificity and affinity. First, the SELEX process starts by incubating target molecules with a pool of oligonucleotides to yield binding complexes in a binding buffer. Second, the unbound oligonucleotides are separated from the binding complexes using different methods, depending on a specific type of SELEX. Third, elution of binding oligonucleotides from the complexes is carried out. Fourth, to increase the quantity of binding sequences, the oligonucleotides are amplified: DNA binders use polymerase chain reaction (PCR), while RNA binders use reverse transcriptase polymerase chain reaction (RT-PCR). Finally, the amplified

sequences are used as the new library to begin the next cycle of the SELEX process. This cycle is repeated for 8 – 12 rounds which could yield the sequences, that can attach to the target with great precision and strength. Then, the binding pools are cloned and verified their sequences.

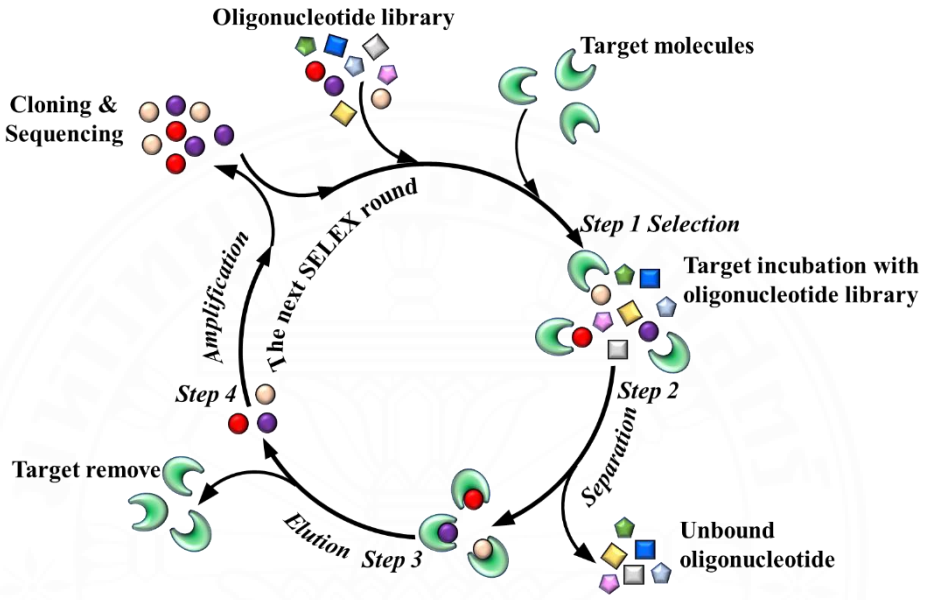

Fig. 2.1 Schematic of Systematic Evolution of Ligands by Exponential Enrichment (SELEX)

Aptamers have been used as binding ligands for enormous applications including cancer diagnosis, therapeutics, cell imaging, drug delivery, biosensing, and function regulation.

2.2.2 Aptamer-functionalized DNA nanostructures for cancer therapy

With their small size, easy modification, and nontoxic nature, aptamers are ideal candidates for targeted cancer therapy. Their high target specificity makes them particularly effective [44]. The combination of DNA nanostructure and functional DNA molecules could provide tools for delivering therapeutic molecules to target cells. In this regard, the aptamer-functionalized DNA nanostructure has drawn much interest.

2.2.2.1 Targeted drug delivery

Many drugs currently used in the clinic can't tell the difference between diseased and healthy cells. This results in them not only attacking the intended target but also damaging healthy, fast-growing cells. A major focus in drug development must be to create more precise therapeutic agents. In the past decade, targeted therapy that is able to specifically deliver drugs or biological agents yielding accumulation of the drugs in diseased sites have been investigated numerously [45-47]. The results showed an increase in selectivity of therapeutic effects but decrease in the adverse effect. The ability of aptamers to precisely recognize proteins on cell membranes and in the blood makes them promising candidates for new therapies [48, 49].

The DNA nanostructure modification using a ligand or transfection agent improved the target specificity and cellular uptake. For instance, folate conjugated DNA was internalized at the specific cellular location [26, 50-52]. In recent years, researchers have been developing and modifying aptamer nano-drug delivery systems to improve treatment effectiveness and reduce unwanted side effects. Seeman proposed the idea of DNA assembly into a branched structure that has drawn much attention in the field of DNA nanostructures. He designed a four-way junction, which connected the DNA to form the extended nanostructures with controllable spacings and repeatable patterns. The sticky end was designed as a hybridization site at the end of two single-stranded DNAs for forming self-assembly structures [53]. This simple idea has been used as an innovative strategy for development of DNA self-assembly. For example, Lin et al. created a nanomedicine platform by building a DNA tetrahedron from the AS1411 aptamer and the anticancer drug 5-fluorouracil (5-FU). Subsequently, cellular uptake was compared between breast cancer cells and normal breast cells, revealing markedly higher uptake in the cancer cells relative to their normal counterparts. Their results demonstrated that this nanomedicine markedly outperformed free 5-FU, exhibiting substantially enhanced therapeutic efficacy in target cells [54]. Moreover, the modification of DNA nanostructure significantly enhanced the drug loading capacity. Tan et al. developed aptamer-tethered DNA nanotrains (aptNTrs), which are DNA-based nanostructures functionalized with aptamers to enable targeted delivery of anticancer drugs. The aptamers guide the nanotrains to specific cancer cell surface markers, enhancing selective uptake and

therapeutic efficacy while minimizing off-target effects. SCG8 aptamer was a navigator that guided the nanotrains toward targeted cancer cells. The long double-strand DNA functioned as a cargo for drug loading. Their results showed that aptNTrs had potential antitumor properties and un-detectable side effects [55]. Bermudez H. and Charoenphol P. incorporated AS1411 aptamer to DNA pyramids. Without transfecting agent, these structures showed more resistance to nuclease degradation than the single stranded aptamer, enhanced intracellular uptake of Hela cell and selectively inhibited the cell growth [56]. Aptamer-functionalized DNA nanostructures present multiple advantages for cancer therapy: their high drug-loading capacity allows efficient delivery of therapeutic agents, excellent biocompatibility minimizes toxicity to normal tissues, and specific target recognition ensures selective interaction with cancer cells, thereby enhancing treatment efficacy and reducing off-target effects. The DNA could also be conjugated with chemotherapeutic agents (e.g. Dox) via covalent [57] and noncovalent [58] bonding. AS1411 aptamer is the most used in targeted drug delivery.

2.2.2.2 Aptamer – drug conjugates

The conjugation of targeting ligands with therapeutic drugs at carefully optimized stoichiometric ratios has garnered significant attention, as it enhances selective drug delivery, improves pharmacological efficacy, and provides a framework for rigorous drug quality control and characterization. For instance, aptamers as recognizing elements were coupled with anti-cancer drugs resulting in effective chemotherapeutic agents. Sullenger et al. engineered tunable cytotoxic agents, termed ApDCs, E3 aptamers conjugated to the highly potent chemotherapeutics monomethyl auristatin E (MMAE) and monomethyl auristatin F (MMAF), enabling targeted delivery and controlled cytotoxicity compared to the unconjugated drugs. *In vitro* studies demonstrated that these conjugated drugs were specifically internalized by prostate cancer cells, resulting in efficient cell killing [59]. Rossi et al. developed a pancreatic cancer–specific RNA aptamer, P19, which was conjugated with multiple chemotherapeutic agents—5-fluorouracil (5-FU), monomethyl auristatin E (MMAE), and a maytansine derivative (DM1)—to enable targeted and multifunctional cytotoxicity. Phosphorylation of histone H2AX at Ser139 was induced by these ApDC complexes, leading to a marked inhibition of PANC-1 and AsPC-1 cell proliferation, while maintaining minimal cytotoxicity in normal cells [60]. Aiming to address drug-

resistant cancers, Chu et al. designed a nanocarrier constructed from DNA origami. The nanocarrier was designed to combine chemotherapeutic and gene-silencing functions, comprising Dox and two antisense oligonucleotides targeting P-glycoprotein (P-gp)and B-cell lymphoma 2 (Bcl-2), and the MUC1 aptamer for enhancing specificity of the cancer treatment [61]. Moreover, incorporation of different prodrugs that have distinct pharmacological mechanisms to the aptamers is a promising rationale for a targeted combination therapy. The circular bivalent aptamer (cb-apt), as demonstrated by Tan et al., exhibited strong binding affinity along with enhanced thermal stability and nuclease resistance. Therefore, the synthesis of ApDCs is a feasible strategy for the incorporation of multiple drugs which shows benefits for targeted therapy [62].

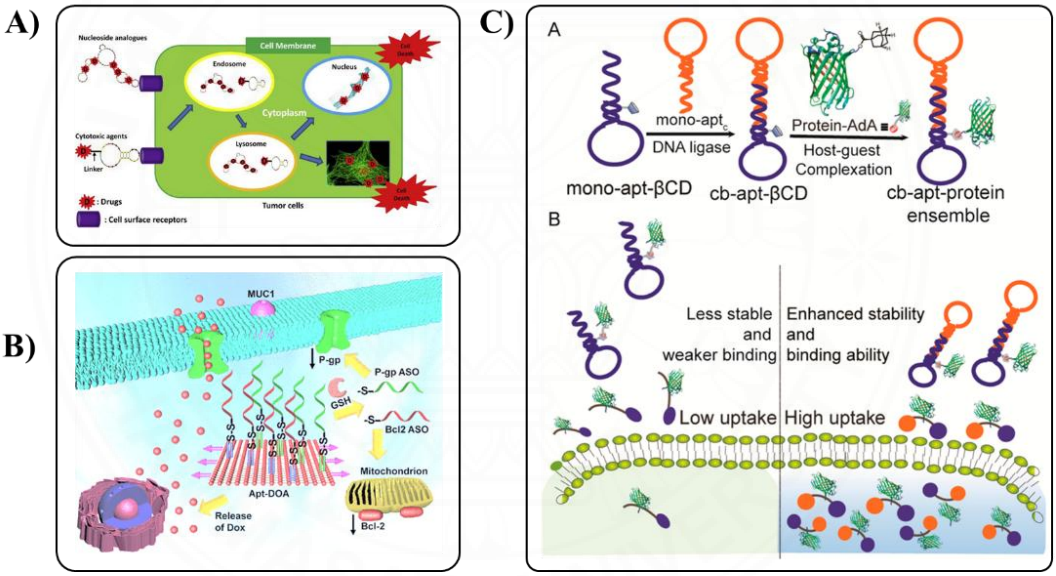

Fig. 2.2 The role of nanostructures engineered through DNA origami in delivering targeted treatments to tumors. A) P19 aptamer–drug conjugates selectively inhibited pancreatic cancer cells by inducing DNA damage with minimal toxicity [60]. B) DNA origami nanocarrier enhanced targeted therapy by delivering Dox and antisense agents to cancer cells [61]. C) The aptamers possess strong stability and resistance, supporting ApDCs as an effective strategy for multi-drug targeted therapy [62].

2.2.2.3 Aptamer as carriers for ASOs

The ASOs were first published in 1970s for therapeutic application [63]. ASOs are short single-stranded chemically synthesized oligonucleotides which form specific Watson-Crick base pairing to target complementary mRNAs resulting in the mRNA destabilization and translation interference. There are two main processes of ASO interference mechanism: RNA-degradation and steric blocking. First mechanism involves ASOs binding to mRNAs, which blocks ribosomes from translating proteins. Second mechanism, ASOs facilitate mRNA degradation similar to endogenous nucleases [64]. Thus, ASOs are a promising therapeutic option for cancer therapy because they can precisely manipulate gene expression. However, ASOs have limitations on delivery and cellular uptake issues. ASO–aptamer conjugation was applied to enhance delivery efficiency and target engagement by improving molecular stability and binding specificity. This method could reduce ASO dosage and off-target effect and enhance cytocompatibility. For instance, Pei and colleagues prepared a hybrid molecule, or chimera, consisting of an aptamer and an antisense oligonucleotide (AS). This chimera was designed to silence the galectin-1 gene, which is overexpressed in tumors. The results showed that Apt-AS entered the cell through endocytosis pathway with acceptable antisense gene silencing efficiency [65]. Furthermore, the cellular uptake and selectivity were reported to be improved. Obika et.al. created the aptamer-ASO for A549 cell uptake. They found that the aptamer-ASO conjugate has potential activity on endosomal/lysosomal escape due to the addition of chloroquine [66]. In addition, the easy modification of ASOs with aptamers could extend the body circulation time (eg. longer half-life). Zhu et.al. prepared nucleic acids (LNAs) targeting viral non-structural protein 9 (NSP9) with additional short ASOs. By introducing a methylene bridge between the 2′-O and 4′-C positions of the sugar ring, the modification enhanced both thermal stability and resistance to nuclease degradation. Moreover, this molecule showed inhibition of porcine reproductive and respiratory syndrome [67].

2.2.2.4 Aptamer as carriers for siRNA

The antisense RNA was first introduced by Fire and Mello in 1998 [68]. Since then, it altered researcher understanding of gene regulation which could revolutionize the research in biological fields. Structurally, siRNA is a short double-

stranded RNA. It downregulates a specific target by degrading mRNA and inhibiting translation. siRNA has been applied for therapeutic gene silencing resulting in high treatment efficiency. However, owing to its hydrophilic properties, naked siRNA has limitation on cellular uptake and internalization. Moreover, it is susceptible to endogenous nuclease degradation upon the exposure of serum proteins which could compromise the efficient tissue and cellular delivery [69]. Conjugating siRNAs with specific molecules offers a promising strategy to overcome the limitations of naked siRNA, enabling improved delivery to target cells or tissues [70]. Aptamers are therefore promising candidates for siRNA conjugation, as they facilitate targeted cellular delivery and promote efficient internalization of siRNA molecules. Generally, aptamer-siRNA conjugates are typically made by combining a siRNA with an aptamer. Aptamers can specifically recognize and bind to target molecules—like cell receptors or integrins—that are located on the surface of a cell, and could facilitate endocytosis for effective delivery of siRNA molecules. In endosomes, the aptamers are removed from conjugated molecules, while the sRNAs are intact and they further induce gene silencing. The conjugation strategy was reported by Chu T.C et.al. and McNamara JO et.al. in 2006. They used different aptamer sequences against prostate-specific membrane antigen (PSMA). Chu, T.C. developed a conjugated molecule by combining two biotinylated A9 anti-PMSA aptamers with two biotinylated siRNAs. These siRNAs were designed to target either glyceraldehyde 3-phosphate dehydrogenase (GAPDH) or lamin A/C [71]. At almost the same time, McNamara covalently attached siRNAs targeting polo-like kinase 1 (PLK1) and B-cell lymphoma 2 (BCL-2) to the 3′-terminus of the PSMA aptamer A10, followed by annealing of the guide strand to form the aptamer–siRNA conjugate. In this study siRNAs have been defined as passenger strands [72]. This aptamer-siRNA conjugate was further tested its activity in an *in vivo* environment [73]. The conjugate was also optimized by sequence truncation, and PEG-tail addition at 3′-end. Following systemic administration, this molecule exhibited cytotoxic effects specifically on PSMA-expressing tumors. Wullner et.al. developed a conjugate composing of PSMA aptamer and mRNA inhibiting Eukaryotic Elongation Factor 2 (EEF2). This conjugate induced specifically prostate cancer cells to undergo apoptosis and cell death [74]. Janne P.A. and Chong C.R. used PSMA aptamer to create a more complex molecule composing of a bivalent PSMA aptamer and two siRNA

against *EGFR* and surviving genes. These two target genes are important oncogenes involving in multiple pathways of cancer. This complex molecule effectively blocked EGFR-mediated angiogenesis and markedly suppressed metastatic progression in prostate cancer [75]. For breast cancer, Liu et al. developed a trivalent chimera siRNA capable of concurrently targeting human epidermal growth factor receptor 3 (*HER3*), human epidermal growth factor receptor 2 (*HER2*), and epidermal growth factor receptor (*EGFR*), providing a multifunctional approach to modulate key signaling pathways in cancer. This chimera has several advantages: minimal immunogenicity, ease of production, high thermal stability, and potent biological activity [76]. To target lung cancer metastasis and suppress epithelial–mesenchymal transition, Peck K. et al. utilized two nucleolin aptamer–siRNA chimeras, aptNCL-SLUGsiR and aptNCL-NRP1siR, effectively blocking critical signaling pathways. The aptNCL–siRNA chimeras selectively and effectively suppressed the expression of SLUG and neuropilin 1 (NRP1) in cancer cells expressing nucleolin, demonstrating both target specificity and functional potency [77]. These studies highlight siRNA as a promising therapeutic, with diverse delivery systems developed to overcome the extracellular and intracellular barriers of *in vivo* applications.

2.2.2.5 Aptamer as carriers for microRNA

microRNAs (miRNA), discovered in 1980, are available throughout the genome and regulate the gene expression in human [78, 79]. Facilitated by RNA polymerase II, microRNAs (miRNAs) are first transcribed as long primary transcripts (pri-miRNAs). These are subsequently cleaved into precursor miRNAs (pre-miRNAs) and further processed to yield mature miRNAs, which play critical roles in post-transcriptional gene regulation [80]. The overexpression of miRNAs associates with many human diseases [81]. Widely studied for their diagnostic potential, extracellular miRNAs have emerged as biomarkers for diverse human diseases, especially cancers, while also functioning as mediators of cell–cell communication [82, 83]. For this reason, miRNAs mimics are developed for using in therapeutic applications. However, they have limitation on specific delivery within the cells [84]. To cross the cellular barrier and improve specificity, drug delivery systems based on miRNA and aptamer have been developed [85]. Aptamer–miRNA conjugates, generated via covalent or non-covalent methods, showed promising activity *in vitro* and *in vivo*. For example, Wu et al.

developed a therapeutic conjugate consisting of the A10-3.2 aptamer linked to miR-15a and miR-16-1, which, when tested in prostate cancer models, effectively induced cancer cell death *in vitro* [86]. Francis et al. explored multiple strategies for delivering miRNAs using the GL21.T aptamer in glioblastoma and non-small cell lung cancer (NSCLC). By selectively binding to the AXL receptor on NSCLC cells, the aptamer not only facilitated targeted delivery but also effectively inhibited receptor activity. Three GL21.T-based conjugates—GL21.T–let-7g, GL21.T–miR-212, and GL21.T–miR-34c—were designed and evaluated in NSCLC cells. Notably, GL21.T–let-7g delivery to A549 cells led to increased let-7 levels and consequent suppression of its target, high-mobility group AT-hook 2 (HMGA2). The *in vivo* study was further investigated using A549 tumor-bearing immunodeficient mice and confirmed the *in vitro* results [85, 87]. Condorelli et.al. used the same approach to prepare GL21.T -miR-34c conjugates. They demonstrated that their conjugates affected NSCLC proliferation because the conjugate targeted AXL receptor and consequently provided the acquired RTK-inhibitor resistance. By targeting the AXL receptor, the GL21.T–miR-34c conjugate effectively suppressed NSCLC cell migration and viability while enhancing their sensitivity to erlotinib [88]. Additionally, the GL21.T-miR-212 chimera made AXL-positive NSCLC cells more sensitive to TNF-related apoptosis-inducing ligand (TRAIL). This increased sensitivity was due to the ability of miR-212 to downregulate the expression of the phosphoprotein enriched in diabetes (PED) [89-91].

To specifically target colon carcinoma, Goel et al. focused on colon cancer–associated miRNAs to enable targeted strategies and identified miR-139-5p as a reliable biomarker, effectively indicating tumor recurrence and metastatic potential [92]. Liang et al. prepared cationic liposome-based nanoparticles integrated with miR-139-5p and modified surface with an aptamer binding to epithelial cell adhesion molecule (EpCAM) [93]. The nanoparticles were applied for colorectal therapeutics. These nanoparticles demonstrated potent anticancer activity by suppressing invasion, migration, and proliferation across multiple colorectal cancer cell lines. Elmi et al. engineered AS1411 aptamer–let-7d miRNA conjugates using two different linking strategies and evaluated their impact on MKN-45 gastric cancer cell proliferation. The results demonstrated that the aptamer–let-7d miRNA conjugate exhibited a stronger

antiproliferative effect on gastric cancer cells compared with the non-conjugated aptamer. This aptamer conjugate showed its potential on cancer treatment [94].

2.2.3 AS1411 Aptamer-based targeted delivery

AS1411 aptamer, a DNA sequence with 26-mer G-rich region,[16, 17] was conjugated with drugs and named as AS1411-DCs. AS1411 aptamer functioned as a recognition ligand for nucleolin that overexpressed on cancer cell's surface. The drugs showed their capability to inhibit or damage cancer cells. For example, Cruz et.al. studied AS1411 aptamer as a macromolecular carrier for an acridine drug and tested this developed G- quadruplex aptamer with HeLa cells. The results showed that the complex of AS1411-C_8 had high binding strength and low cytotoxicity toward non-malignant cells [95]. Abnous et.al. reported a three-way junction DNA nanostructure with three AS1411 aptamer strands loaded with doxorubicin (Dox) for targeted cancer therapy. AS1411 aptamer worked as targeting nucleolin and therapeutic activity toward biomarkers of prostate (PC-3 cells) and breast (4T1 cells) cancers. It showed that the cellular uptake was preferable in target cancer cells. Furthermore, Dox-loaded three-way junction DNA nanostructure displayed enhanced serum stability and pH-responsive behavior. In vivo, it more effectively suppressed tumor growth compared with free Dox. These findings suggest that the DNA nanostructure could mitigate the adverse effects of Dox on surrounding healthy cells [96]. Biocca et.al. prepared an octahedral DNA nanocage carrying AS1411 aptamer (Apt-NC) that had selective effects on target cancer cells resulting in anti-tumor activity. Apt-NC was stable in serum and its anti-cancer activity was 200-fold greater than the free aptamer. Cellular uptake study of Apt-NCs structure revealed that the nanostructure entered to the cells through the endo-lysosomal pathway, since it was not detected in nuclei. Observations revealed that free AS1411 aptamer primarily accumulated in the perinuclear region and within nucleoli [97]. These studies showed that the AS1411 aptamer coupled with different nanomaterials had attractive characteristics including selectivity and specificity toward targeted cancer cells. AS1411 aptamer-based delivery systems offer several advantages, including high nuclease resistance, prolonged in vivo circulation, and enhanced therapeutic efficacy.

2.3 T9/U4 antisense oligonucleotide

T9/U4 ASO with a sequence of 5′-TAGGGTTAGACAA-3′ has been reported as a complementary to the template of telomerase RNA [22]. The sequence of T9/U4 with the length of 13mer and 15mer had less effective on reducing telomerase activity [98]. The T9/U4 modification with phosphorothioate bond (PS) provided certain characteristics of this ASO as enhancing efficiency but decreasing selectivity. Thus, the integration of this ASO with a recognition molecule such as aptamer is a promising strategy on developing the complex with high specificity and affinity.

2.4 Doxorubicin (Dox)

Doxorubicin (Dox), an anthracycline (
Fig. 2.), is an anticancer drug widely used in chemotherapy. It was discovered as an anticancer drug derived from actinobacteria *Streptomyces peucetius*. The mechanism of action was reported in 1969 [99]. In 1974, it was approved by USFDA for a clinical treatment for various cancers, and had a commercial name as Adrymicin [100]. Key mechanism is as follows. Dox induces DNA damage in cancer cells. The intercalation of Dox in DNA double helix causes inhibition of topoisomerase II [101, 102]. Mejia et.al studied the interaction pathway of Dox and energy source molecules such as adenosine triphosphate (ATP) and guanosine triphosphate (GTP) to acquire more insight about the effect of Dox on these molecules. They found that Dox bound to these molecules in the sub-millimolar range of dissociation constant (K_d), indicating that these energy molecules are one of Dox target inside the cells [103]. However, therapeutic usage of Dox has been obstructed by cardiotoxic side effects, including dilated cardiomyopathy [104] and congestive heart failure[5]. These adverse effects depend on dose and duration of treatment. Several treatment strategies have been developed to reduce Dox-mediated cardiotoxicity, such as lowering the dosage of drug and combining it with DNA duplex. The advantage of Dox intercalation into DNA inspires a researcher to develop the approach for minimizing the Dox side effect. Rotkrua et.al. formed Dox-loaded aptamer, they found that the DNA duplex significantly reduce Dox cytotoxicity in C cells when compared with the complex without Dox [105]. Li et.al. demonstrated that

the complex of L33 aptamer-Dox has high specificity and affinity (K_d = 14.3 ± 2.2 nM) to HCT116 cells. This complex had less cytotoxicity on CL187, non-target cells, indicating its selective drug delivery to the target cells [106]. Furthermore, Bavi et.al. observed that the conjugation between Dox and 16-mer DNA reduces adverse effect of and significantly enhanced cellular uptake *in vivo* [107]. These findings demonstrated that Dox delivery systems based on aptamers could overcome drug resistant issues and have potential in clinical application, because high drug dosages are applied directly to the target cells.

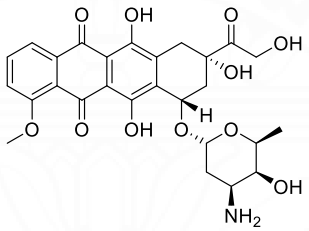

Fig. 2.3 The chemical structure of doxorubicin.

2.5 Mitoxantrone (MTZ)

Mitoxantrone (MTZ) is a potent synthetic anthracenedione agent that fights cancer through several mechanisms. Its primary functions are to intercalate into DNA and inhibit topoisomerase II, an enzyme that is vital for DNA replication and repair [108]. This results in DNA strand breaks, disrupting cell proliferation and inducing apoptosis in rapidly dividing cancer cells. Initially developed as a less cardiotoxic alternative to anthracyclines like doxorubicin, mitoxantrone has shown efficacy against a variety of malignancies, including acute myeloid leukemia (AML), advanced hormone-refractory prostate cancer, breast cancer, and non-Hodgkin's lymphoma [109-111]. It is also utilized in the management of multiple sclerosis, particularly in worsening relapsing-remitting and secondary progressive forms, due to its immunosuppressive properties. Clinically, mitoxantrone is typically administered intravenously and often used in combination regimens with other chemotherapeutic agents to enhance its therapeutic effect. Its use is associated with a well-documented toxicity profile, the most significant of which

includes dose-dependent cardiotoxicity, manifesting as a decline in left ventricular ejection fraction and, in severe cases, congestive heart failure[112, 113]. Other common adverse effects include myelosuppression, nausea, alopecia, and mucositis. Despite its effectiveness, the risk of secondary malignancies, such as therapy-related acute leukemia, has been reported, particularly with prolonged use. The drug's pharmacokinetic properties, including a large volume of distribution and extensive tissue binding, contribute to its prolonged biological activity but also complicate dosing schedules. In terms of molecular structure, mitoxantrone features planar aromatic rings that facilitate its DNA intercalation [114], and its synthetic derivation allows for structural modifications aimed at enhancing therapeutic index and minimizing side effects (**Fig 2.3**). Ongoing research focuses on improving its delivery via nanoparticle formulations or liposomal encapsulation to increase tumor selectivity and reduce systemic toxicity [115]. Moreover, studies are investigating mitoxantrone's role in overcoming multidrug resistance mechanisms, especially in solid tumors, by modulating drug efflux transporters. Resistance to mitoxantrone, often mediated by overexpression of ABC transporters such as BCRP (breast cancer resistance protein) [116, 117], remains a clinical challenge and a subject of current investigation. Additionally, mitoxantrone's immunomodulatory effects have prompted exploration into its synergistic potential with immune checkpoint inhibitors in various oncologic settings [118]. While newer targeted therapies and immunotherapies are reshaping the landscape of cancer treatment, mitoxantrone retains a niche in certain refractories or relapsed malignancies, where its broad cytotoxic profile can still offer meaningful clinical benefit. In summary, mitoxantrone remains a valuable, albeit carefully monitored, component of the oncologic pharmacopeia, with a legacy of utility in both hematologic and solid tumors, as well as non-oncologic immune-mediated diseases. Continued research into mitigating its toxicities while enhancing its efficacy could further optimize its role in contemporary cancer therapy.

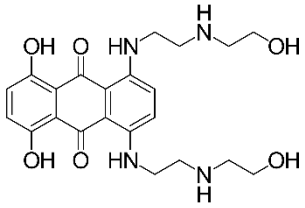

Fig. 2.4 The chemical structure of mitoxantrone.

2.6 T4 DNA ligase

DNA ligases were found in all living cells. They facilitate DNA replication, repair, and recombination by forming phosphodiester bonds between adjacent 3′-OH and 5′-phosphate ends in dsDNA [119]. T4 DNA ligase is widely used because of the efficient joining of blunt-ended dsDNA. The ligation reaction proceeds through three sequential steps of nucleotide transfer. The first step, enzyme adenylation undergoes the formation of a covalent protein – AMP intermediate resulting in pyrophosphate (PPi) release. Second, the AMP was transferred to the 5′-phosphate at the nick site to form DNA-adenylate. In the last step, 3′-OH of the nick site attacks 5′-phosphate to form a phosphodiester bond [119] (**Fig 2.4**). Lund et.al. developed a simple protocol based temperature-cycling ligation for DNA cloning using T4 DNA ligase. This protocol was carried out at a following condition; 200ng DNA, 0.1 Weiss/10 μL T4 DNA ligase, and T4 buffer. The temperature was periodically programed to be 10°C for 30s and 30°C for 30s. The ligation was incubated in this temperature program for 12-16 hours. They found that cloning efficiency of sticky-end and blunt-end were increased to 4-8-fold and 4-6-fold, respectively [120]. Zhang et.al. developed a technique based on real-time polymerase chain reaction for quantitatively analyzing sensing signals from interaction between ATP and T4 DNA ligase and used this developed technique for detecting ATP in living cells. Two short oligonucleotides were linked together through T4 DNA ligase when ATP presented in the system [121]. Wang et.al studied the DNA repairing through the T4 DNA ligase on the irradiated cells *in vivo*. The *in vivo* result indicated that T4 DNA ligase contributed to a repairing of DNA double strand fragment [122].

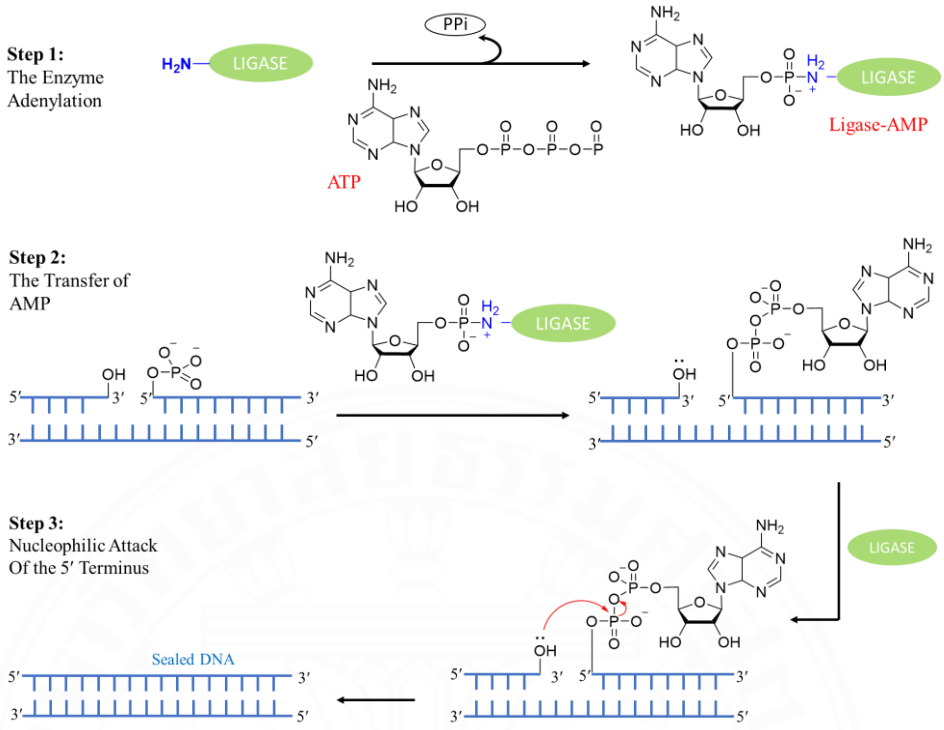

Fig. 2.5 Schematic reaction of T4 DNA ligase.

CHAPTER 3
RESEARCH METHODOLOGY

3.1 Reagent

DNA molecules (Table 3.1) were obtained from Integrated DNA Technologies (IDT), and all chemicals used are listed in Table 3.2

Table 3.1 The DNA sequence used in this study.

Name	**Sequence (from 5′ to 3′)**
AS-wagon	Phos-TAG ATT GTT AGA TTG TTT TTG GTG GTG GTG GTT GTG GTG GTG GTG GTT TTT GAG AGT GAT AGA TGG
CT-wagon	Phos-TAG ATT GTT AGA TTG TTT TTG TGT GGG GGT GGG TGG TGT GTG GTT GTT TTT GAG AGT GAT AGA TGG
Bogie	CAA TCT AAC AAT CTA CCA TCT ATC ACT CTC
FAM-Bogie	FAM-CAA TCT AAC AAT CTA CCA TCT ATC ACT CTC
Hybridization strand (HBS)	GAG TAT CCG TGT AAT GTG CTG ACA GAT CGA GCT TCG ATA GCC GAT
CT-AS1411-HBS	TTC CTC CTC CTC CTT CTC CTC CTC CTC CAT CGG CTA TCG AAG CTC GAT
AS1411-HBS	GGT GGT GGT GGT TGT GGT GGT GGT GGC CAT CGG CTA TCG AAG CTC GAT
T9/U4-HBS	AGC ACA TTA CAC GGA TAC TCC CTA GGG TTA GAC AA
FAM-T9/U4-HBS	FAM-AAG CAC ATT ACA CGG ATA CTC CCT AGG GTT AGA CAA
CT-T9/U4-HBS	AGC ACA TTA CAC GGA TAC TCC CAT TAC AGT GAG AG

Table 3.2 The chemical used in this study

List of chemicals	Supplier
Acrylamide/Bis-Acrylamide solution 30% (29:1)	Hi-Media, India
Acrylamide/Bis-Acrylamide solution 30% (19:1)	Hi-Media, India
Annexin V FITC/PI apoptosis detection kit	Dojindo, Japan
Ammonium persulfate	LOBA
BCA protein assay kit	Thermo Sciencetific, USA
4′,6′-diamidino-2-phenylidoledihydrochloride (DAPI)	Sigma-Aldrich, USA
Doxorubicin hydrochloride (Dox)	Fresenius Kabi, Thailand
Dulbecco's modified eagle medium (DMEM)	Gibco, USA
Ethylene diamine (EDTA)	Bio-Rad, USA
Fetal bovine serum (FBS)	Gibco, USA
Gel loading buffer	Sigma-Aldrich, USA
Glycine	Bio-Rad, USA
4x Laemmli sample buffer	Bio-Rad, USA
Methanol	LOBA
Mitoxantrone (MTZ)	Sigma-Aldrich, USA
Non-essential amino acid	Gibco, USA
Penicillin-streptomycin (Pen/Strep)	Gibco, USA
Phosphate buffer saline (PBS)	Bio Basic, Canada
Protease inhibitor	Amresco, USA
RIPA buffer	Amresco, USA
Sodium dodecyl sulphate	Bio-Rad, USA
N,N,N,N- Tetramethylethylenediamine (TEMED)	Merck, Germany
Tris base	Bio-Rad, USA
Tris buffer saline (TBS)	Bio-Rad, USA
Tris-borate -EDTA buffer (TBE)	Sigma-Aldrich, USA
Tris(hydroxymethyl)aminomethane hydrochloride	Bio-Rad, USA
Trypsin-EDTA	Gibco, USA
Tween 20	Sigma-Aldrich, USA

3.2 Formation of multifunctional drug delivery system based on DNA aptamer.

3.2.1 Aptamer train formed by hybridization and enzymatic ligation.

The aptamer train (AT) was prepared by the hybridization of two oligonucleotide sequences: AS-wagon and Bogie. To complete the formation of AT the optimal ratio of AS-wagon and Bogie at a molar ratio of 1:3 was used, ensuring that all components could fully react with each other. The complexes were incubated at 90 °C for 5 min. Then the incubation temperature was rapidly cooled down to 0 °C maintained for 5 min. After hybridization, AT was formed via enzymatic ligation facilitated by 400 units of T4 DNA ligase between 5′ and 3′ end of AS-wagon in a ligation buffer containing 50 mM Tris-HCl, 10 mM $MgCl_2$, 10 mM DTT, and 1 mM ATP at 25°C. The ligation was carried out overnight before thermally inactivating the ligase at 70 °C for 10 min. AT was verified by 10%/20% stacked polyacrylamide gel electrophoresis. For a control train (CT), AS-wagon sequence was replaced by a scrambled sequence. For further experiments these complexes was used without purification.

3.2.2 A molecular hybrid composing of AS1411 aptamer and T9/U4 ASO (AS-T9/U4_MH)

T9/U4-HBS, AS1411-HBS, and HBS (10 μM each) were mixed in PBS solution and incubated 24 h at room temperature. The molecular hybrid was confirmed by 10%/15% polyacrylamide gel electrophoresis. This molecular hybrid was named as AS-T9/U4_MH. In addition, two control molecular hybrids were prepared by replacing T9/U4 ASO and AS1411 aptamer with two scrambled sequences and were named as AS-nonT9/U4_MH, and nonAS-T9/U4_MH, respectively.

3.3 Cell culture

Colorectal adenocarcinoma cell lines B and C, along with normal colon cells A, were purchased from ATCC (USA). Cells were maintained in DMEM supplemented with 10% fetal bovine serum and 1% penicillin–streptomycin at 37 °C under a 5% CO_2 atmosphere. For B cells, the medium was further supplemented with non-essential amino acids. Cultures were passaged upon reaching 70–80% confluence.

3.4 Activity study of MH *in vitro*

3.4.1 Stability and binding of MH *in vitro*

T9/U4-HBS was 5′-labeled with carboxyfluorescein (FAM) for fluorescence detection by microscopy and flow cytometry.

3.4.1.1 Fluorescence microscope

After seeding A normal colon cells and B and C cancer cells in 96-well plates (3×10^5 cells/well) and culturing for 24 h, the cells were exposed to 10 μM FAM-labeled AS-T9/U4_MH or nonAS-T9/U4_MH for 1.5 h. After treatment, the culture medium containing the compounds was carefully aspirated, and the cells were gently rinsed twice with sterile phosphate-buffered saline (PBS) to remove any residual treatment agents and unattached molecules. Each washing step was performed by adding an appropriate volume of PBS to fully cover the cell monolayer, followed by gentle aspiration to avoid disrupting the cells. This washing procedure ensured that only the internalized or specifically bound molecules remained associated with the cells for subsequent analyses. Following the washing steps, the cell nuclei were stained with 4′,6-diamidino-2-phenylindole dihydrochloride (DAPI) to enable visualization of nuclear morphology. The staining was carried out by incubating the cells with DAPI solution for a defined period under dark conditions to prevent photobleaching. Excess dye was removed by rinsing with PBS, ensuring clear nuclear contrast. Finally, the stained cells were observed and imaged using a confocal laser scanning microscope (CLSM, ZEISS CLS 900), which allowed high-resolution acquisition of both fluorescence signals and detailed cellular structures.

3.4.1.2 Flow cytometry

Flow cytometry was used to measure single cells in a fluid stream through lasers to detect fluorescence intensity that it can bind to the cell. In the experiment, A, B, and C cells were seeded into 12-well plates at a density of 3×10^6 cells per well and incubated for 24 h to allow cell attachment and recovery. The cells were then exposed to 5 μM of the designated molecular hybrid (MH) under standard culture conditions. Following treatment, the culture medium was removed, and the cells were gently washed twice with sterile PBS to eliminate any unbound compounds. The cells were subsequently detached by trypsinization, collected, and washed two

additional times with PBS to ensure removal of residual trypsin and extracellular molecules. Finally, the cell pellets were resuspended in 0.5 mL of PBS and subjected to binding analysis using a CytoFLEX flow cytometer (Beckman Coulter)).

3.4.2 Cell proliferation assay

The cells were treated with AS-T9/U4_MH, AS-nonT9/U4_MH, and nonAS-T9/U4_MH. After 48 hours of incubation, the MTS reagents were used to determine cell proliferation. The cell viability was compared with cell viability of untreated cells.

3.4.3 Incorporation of Dox into MH

Intercalation was a key strategy for incorporation of Dox into MH. In brief, the IC_{50} value of Dox at 0.95 μM was incubated in10 μM of MH at room temperature in the dark for 1.5 h. The Dox intercalation was characterized by measuring fluorescence signal of intercalated Dox using a fluorescence microplate reader (Varioskan, Thermo Scientific, USA). The excitation wavelength was set at 480 nm and emission wavelengths were recorded from 500 to 800 nm. Dox incorporated MHs were named as Dox-loaded AS-T9/U4_MH, Dox-loaded AS-nonT9/U4_MH, and Dox-loaded nonAS-T9/U4_MH.

3.4.4 A standard curve of Dox

A various concentration of Dox (0.95, 0.48, 0.24, 0.12, 0.06, 0.03, and 0.015 μM) were prepared in deionize water and measured fluorescence intensity at 590 nm after excited at 480 nm using fluorescence microplate reader.

3.4.5 Dox loading

A fixed molar ratio at 1:0.095 of AS-T9/U4_MH to Dox was prepared in different concentrations of AS-T9/U4_MH including 5, 10, 15, and 20 μM. At respective Dox concentrations are 0.475, 0.95, 1.9, and 3.8 μM.

3.4.6 AS-T9/U4_MH capacity for Dox loading

Dox at concentrations of 0, 0.95, 5, 10, 20, and 40 μM was added to a 10 μM of AS-T9/U4_MH in PBS. The mixtures were incubated at room temperature for 1.5 hours. After that, the fluorescence intensity of Dox was recorded using a fluorescence microplate reader.

3.4.7 Dox released

At 37°C, Dox-loaded AS-T9/U4_MH was incubated in cell culture medium, and samples were taken at various time intervals—1, 3, 6, 12, 24, 48, and 72 hours. The absorbance of each sample was measured across a wavelength range of 350–800 nm. The absorbance value at 409 nm, representing Dox's maximum peak, was used to quantify the release, with 0.95 μM Dox defined as 100% release.

3.4.8 Stability of MH in the cell culture environment

Following incubation of Dox-loaded AS-T9/U4_MH in cell culture media, samples were collected at different time intervals —1, 3, 6, 12, 24, 48, and 72 h. for electrophoresis analysis. The gel results illustrate the structural changes and stability of the complex over time

3.4.9 Effect of Dox-loaded MH on cell proliferation.

$5x10^3$ cells of C cell, B cell and A cells were seeded into each well of 96-well plates and cultured for 24 h and allowed to adhere and grow for 24 h. Following this incubation, the cells were treated with either 0.95 μM free Dox or 10 μM of Dox-loaded molecular hybrids, including nonAS-T9/U4_MH, AS-nonT9/U4_MH, and AS-T9/U4_MH, under standard culture conditions. Cell proliferation was determined using MTS assay.

3.4.10 Western blot analysis

C cells were exposed to 10 μM of Dox-loaded AS-T9/U4_MH, Dox-loaded AS-nonT9/U4_MH, AS-T9/U4_MH, and AS-nonT9/U4_MH, as well as 0.95 μM free Dox, under standard culture conditions to evaluate their effects on cell viability and drug delivery efficiency. Following treatment, the cells were lysed in ice-cold RIPA buffer supplemented with protease and phosphatase inhibitors to preserve protein integrity. Protein concentrations were determined using the BCA protein assay. For electrophoresis, 50 μg of total protein per sample was loaded onto a 10% SDS-PAGE gel, separated by molecular weight, and subsequently transferred onto PVDF membranes for immunoblotting analysis. The PVDF membranes were blocked with Intercept (TBS) blocking buffer for 1 h at room temperature to prevent nonspecific binding. Subsequently, the membranes were incubated overnight at 4 °C with the designated primary antibodies for target protein detection as follows: Bax (1:1000; 20 kDa, Cell signaling), Bcl–2 (1:1000; 25 kDa, Cell signaling), β- actin (1:1000; 42 kDa,

Abcam), vimentin (cat. no. ab92547; 1:1000; 54kDa; Abcam), and hTERT (cat. no. ab32020; 1:1000; 127 kDa; Abcam). After washing the membranes with 0.1% TBS-Tween-20 to remove unbound primary antibodies, they were incubated with goat anti-rabbit IgG H&L/HRP secondary antibody (1:5000) for 1 h at room temperature. Following additional washes with 0.1% TBS-Tween-20, the protein bands were detected and visualized using the Odyssey XF imaging system (LI-COR).

3.4.11 Cell apoptosis

3 x 10^6 cells of C cells were seeded in 12-well plates and allowed to adhere for 24 h. Then, the cells were treated with 10 μM of Dox-loaded AS-T9/U4_MH, Dox-loaded AS-nonT9/U4_MH, AS-T9/U4_MH, AS-nonT9/U4_MH, and 0.95 μM of Dox for 48 h. After treatment, the cells were harvested and resuspended in 100 μL of binding buffer, followed by incubation with Annexin V-FITC/PI (cat. no. AD10-10; Annexin V-FITC/PI Dual Staining Kit, Dojindo) at room temperature in the dark for 15 min. The stained cells were immediately analyzed using flow cytometry to determine the proportion of apoptotic and necrotic cell populations.

3.5 Activity study of AT *in vitro*

3.5.1 Stability and binding of AT and MH *in vitro*

Bogie sequences were labeled with carboxyfluorescein (FAM) at 5′ end for fluorescence signal detection using microscope and flow cytometer.

3.5.1.1 Fluorescence microscope

Cancer cells (B and C cell) and normal colon cells (A cell) were seeded into 96-well plates at density of 3x10^5 cells per well and cultured for 24 h. Next, 1 μM of FAM-labeled AT and FAM-labeled CT were treated the cell and incubated for 1.5 h. After treatment, the treated medium was removed, and the cells were washed with PBS solution two times. For nuclear visualization, cells were stained with 4′,6-diamidino-2-phenylindole dihydrochloride (DAPI) and subsequently imaged on a ZEISS LSM 900 confocal laser scanning microscope.

3.5.1.2 Flow cytometry

3x10^6 cells of A, B, and C cell were seeded into 12-well plates and incubated for 24 h. Cells were exposed to 0.5 μM FAM-labeled AT or FAM-labeled

CT, after which the medium was discarded and the cells were washed twice with PBS. After trypsinization, cells were harvested, washed twice with PBS, and resuspended in 0.5 mL PBS for binding analysis on a CytoFLEX flow cytometer (Beckman Coulter).

3.5.2 Cytotoxicity assay of mitoxantrone (MTZ)

To assess the cytotoxicity of MTZ on cancer cells (B and C cell), approximately 5×10^3 cells were seeded into 96-well plates and incubated for 24 hours. Following incubation, the cells were treated with varying concentrations of MTZ (0, 0.016, 0.031, 0.063, 0.125, 0.25, 0.5, 1.0, 2.0, and 5.0 μM) and incubated for 48 hours. Cytotoxicity was assessed using the MTS assay. Briefly, 20 μL of MTS reagent was added to each well, and the plates were incubated for 1 h at 37 °C before measuring absorbance. The absorbance at 490 nm was recorded with a Thermo Scientific microplate reader (USA), and IC_{50} values were determined using GraphPad Prism 5.

3.5.3 Incorporation of MTZ into AT

Intercalation was a key strategy for incorporating MTZ into AT. For 1.5 hours, 1 μM of AT was incubated with 0.09 μM of MTZ in the dark at room temperature. MTZ intercalation was characterized by measuring the fluorescence signal of intercalated MTZ using a fluorescence microplate reader (Varioskan, Thermo Scientific, USA). Based on previous reports, the samples were excited at 610 nm, and the corresponding emission maxima were measured at 685 nm [114, 123]. The resulting MTZ-incorporated AT was referred to as MTZ-loaded AT.

3.5.4 MTZ loading capacity into AT

To assess the capacity of AT, 1 μM of AT was incubated with varying concentrations of MTZ (0, 0.1, 1, 5, 10, and 20 μM) in a PBS solution at room temperature for 1.5 hours. MTZ fluorescence was determined using a fluorescence microplate reader, setting the excitation wavelength at 610 nm and recording the emission maximum at 685 nm.

3.5.5 MTZ released

The purpose of this experiment was to quantify the release of MTZ from AT. The MTZ-loaded AT was maintained in cell culture medium at 37 °C, and at predetermined time points (1, 3, 6, 12, 24, 48, and 72 h) samples were collected for analysis. The absorbance of samples was measured across 400–800 nm, and the

maximum at 610 nm was employed to calculate the percentage of MTZ released. A concentration of 0.09 μM MTZ was used as the reference for complete (100%) release.

3.5.6 Effect of MTZ-loaded AT on cell proliferation

5×10^3 cells of A, B, and C cells were seeded into each well of 96-well plates and cultured for 24 hours. The cells were then treated with unligased CT, unligased AT, CT, AT, 0.09 μM MTZ, 1 μM MTZ-loaded CT, MTZ-loaded AT, or left untreated as a control. Following treatment, 20 μL of MTS reagent was added per well, and the plates were incubated for 1 h, after which absorbance at 490 nm was recorded using a microplate reader.

3.5.7 Cell apoptosis

3×10^6 cells of C cells were seeded in 12-well plates and incubated for 24 hours. The cells were then treated with 0.09 μM MTZ, 1 μM CT, AT, MTZ-loaded CT, and MTZ-loaded AT for 48 hours. Following treatment, cells were collected, resuspended in 100 μL of binding buffer with Annexin V-FITC/PI (cat. no. AD10-10; Dojindo), and incubated in the dark at room temperature for 15 min. An additional 400 μL of binding buffer was added to each tube, and the cells were analyzed by flow cytometry.

3.5.8 Western blot analysis

C cells were treated with 0.09 μM MTZ, 1 μM CT, AT, MTZ-loaded CT, and MTZ-loaded AT. After collecting, the cells were lysed in ice-cold RIPA buffer supplemented with protease and phosphatase inhibitors to preserve protein integrity. The total protein concentration of cell lysates was quantified using the BCA protein assay kit following the manufacturer's protocol. A total of 20 μg of total protein was loaded per lane, separated on a 12% SDS-PAGE gel, and transferred to PVDF membranes. After blocking with Intercept (TBS) buffer for 1 h at room temperature, the membranes were incubated overnight at 4 °C with the appropriate primary antibodies against Akt (1:1000, 60 kDa, Cell Signaling), β-actin (1:1000, 42 kDa, Abcam), Bcl-2 (1:1500, 25–28 kDa, Cell Signaling), and Bax (1:1500, 20 kDa, Cell Signaling). Following primary antibody incubation, the membranes were washed with TBS-Tween-20 (0.1%) and subsequently incubated for 1 h at room temperature with goat anti-rabbit IgG H&L/HRP (1:15,000; AB175781, Abcam), before washing again

with TBS-Tween-20 (0.1%). Protein signals were detected with the Odyssey XF imaging system (LI-COR).

3.6 Statistical Analysis.

All data were analyzed using one-way analysis of variance (ANOVA). Experiments were performed with a minimum of three replicates to ensure statistical power. Results are presented as mean ± standard deviation (SD), and differences were considered statistically significant at $P < 0.05$.

CHAPTER 4
RESULTS AND DISCUSSION

4.1 Formation of multifunctional drug delivery system based on DNA aptamer.

4.1.1 Aptamer train by hybridization and enzymatic ligation

The sequence design was described as follows. The hybridization regions of AS-wagon were at the first 20 nt of both 5′ and 3′ ends. The sequence of AS1411 aptamer with the length of 26 nt was in the middle of the AS-wagon strand. At the 5′ end of AS-wagon2, a phosphate group was incorporated and functioned as a linking point for enzymatic ligation. Bogie was designed to be complementary with AS-wagon. The AT was formed via hybridization between AS-wagon and Bogie at 90° C for 5 min. After that, enzymatic ligation with T4 ligase in a T4 DNA ligase buffer was carried out at 22 - 25°C overnight, so that the T4 DNA ligase joins DNA fragments by forming phosphodiester bonds, enabling recombinant DNA construction. The formation of AT was characterized by gel electrophoresis. The results showed that hybridization of AS-wagon and Bogie in the absence of T4 DNA ligase yielded complexes with a low molecular weight, approximately 80 - 100 bp (**Fig 4.1**, lanes 4 and 5). When the hybridization was carried out with the addition of T4 DNA ligase, the complexes with sizes greater than 250 bp were detected (**Fig 4.1**, lanes 6 and 7). This was caused by the enzyme that facilitated the conjugation between 5′ phosphate and 3′ hydroxyl group of the AS-wagon strand.

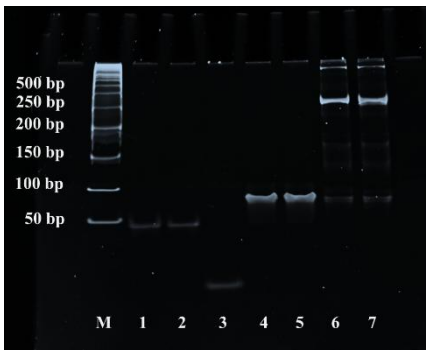

Fig. 4.1 Gel electrophoresis was used to visualize the assembly of AT. The gel was loaded with a DNA marker in Lane M, followed by the individual components AS-wagon in Lane 1, CT-wagon in Lane 2 and Bogie in Lane 3. Lanes 4 and 5 show the hybridization of the two components without T4 DNA ligase, while Lanes 6 and 7 show the hybridization with addition of T4 DNA ligase confirm the successful ligation and formation of the AT complex.

4.1.2 Formation of AS-T9/U4_MH

The antisense oligonucleotide named T9/U4 was reported that it has bioactivity to downregulate expression of human telomerase reverse transcriptase (hTERT) [22]. Hence, MH (composed of AS1411 aptamer and T9/U4 ASO) was prepared via hybridization technique. To facilitate the MH formation, a hybridization strand (HBS) with length of 45 nt served as main skeleton of this molecular assembly. The hybridization regions were the first 20 nt at both 5′ and 3′ ends. Sequences of AS1411 aptamer (AS) and T9/4U ASO (T9/4U) were designed with additional oligonucleotides for forming hybridization with HBS. The MH formation was evaluated using gel electrophoresis. The results demonstrated that there was a distinct, slower-moving bands (top to bottom) when AS and T9/U4 were mixed with HBS. Their sizes were approximately 90 bp interpreted as MH, because the sizes were larger than the size of each building block which confirmed successful hybridization without side products (**Fig. 4.2**).

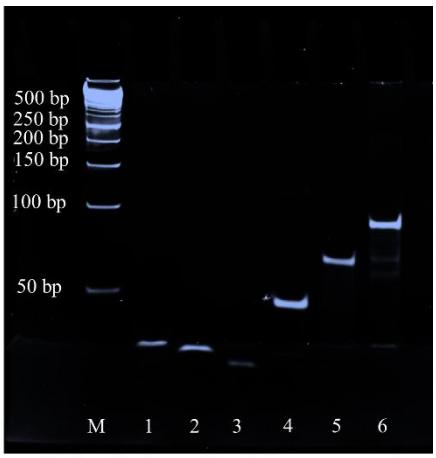

Fig. 4.2 The successful assembly of AS-T9/U4_MH was verified by gel electrophoresis. The gel was loaded as follows: Lane M with a DNA marker; Lane 1 with AS1411-HBS; Lane 2 with HBS; Lane 3 with T9/U4-HBS; Lane 4 with a mixture of HBS and T9/U4-HBS; Lane 5 with a mixture of HBS and AS1411-HBS; and Lane 6 with a mixture of HBS, T9/U4-HBS, and AS1411-HBS [124].

4.2 Activity of AS-T9/U4_MH

4.2.1 Stability and binding of MH *in vitro*.

A fluorescence microscope was used to investigate the capability of AS1411 aptamer as a carrier for T9/U4 ASO and other integrated species to cancer cells. C cells treated with FAM-labeled AS-T9/U4_MH showed brighter fluorescence intensity than B cells and A cells treated with the same molecular hybrid (**Fig 4.3**). It indicated a binding function of AS1411 aptamer that recognizes nucleolin available on the surface of C cells. This result supported the findings from cell viability assay.

To further confirm microscopic results, B and C cells were treated with FAM-labeled nonAS-T9/U4_MH and FAM-labeled AS-T9/U4_MH and detected their fluorescence signals using flow cytometry. The results showed that FAM-labeled AS-T9/U4_MH was able to selectively bind to C cells, since the fluorescence signal collected from cells treated with FAM-labeled AS-T9/U4_MH was significantly higher than that collected from cell treated with FAM-labeled nonAS-T9/U4_MH (**Fig 4.4**). As reported in literatures, AS1411 aptamer exhibits specific binding to nucleolin, a protein highly expressed on the plasma membrane of C cells [105]. Whereas B cells that have less nucleolin availability

exhibited low intensity [125, 126] (**Fig 4.4**). These results confirmed our findings in the microscopic technique.

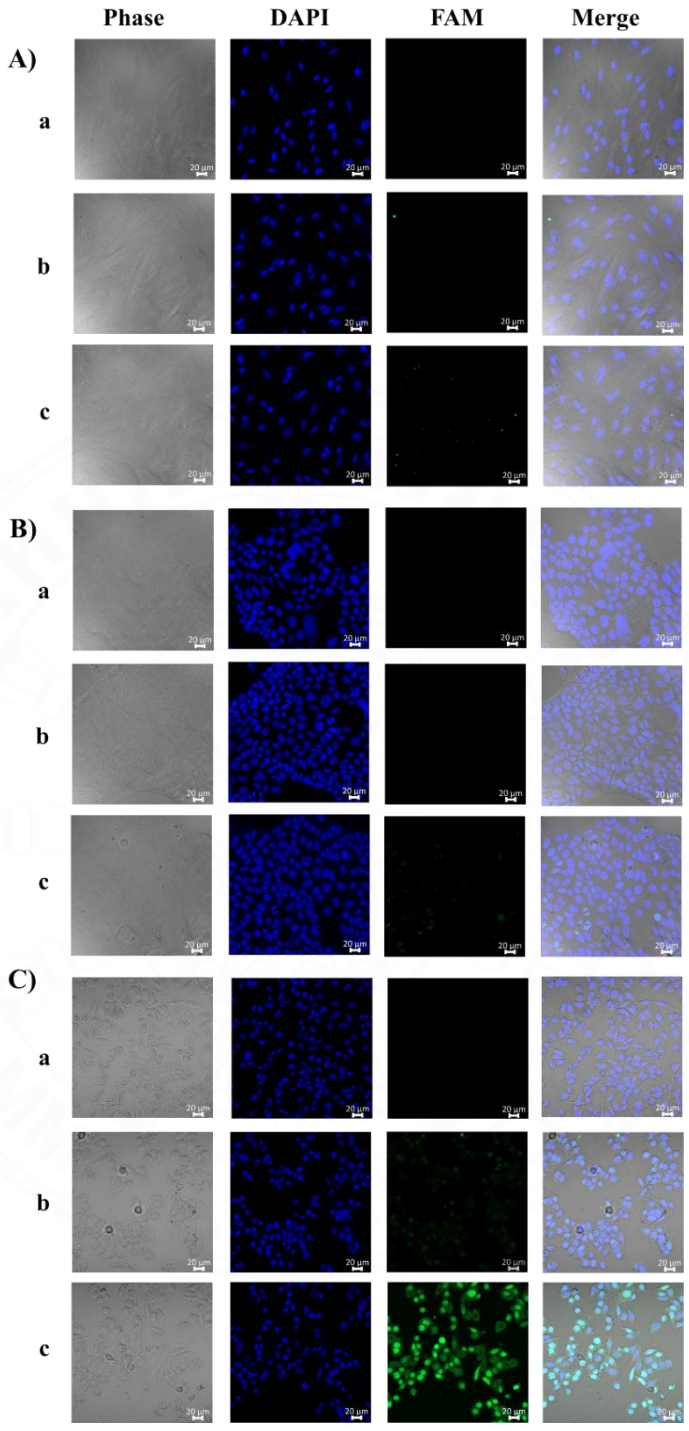

Fig. 4.3 The provided fluorescence images depict the binding and internalization of two different compounds in three distinct cell lines. Panel (A) A cells, (B) B cells, and (C) C cells. Within each panel, sub-image (a) represents untreated as a control, sub-image (b) shows cells treated with a FAM-labeled non-specific molecule (nonAS-T9/U4_MH), and sub-image (c) shows cells treated with the FAM-labeled targeted molecule (AS-T9/U4_MH) [124].

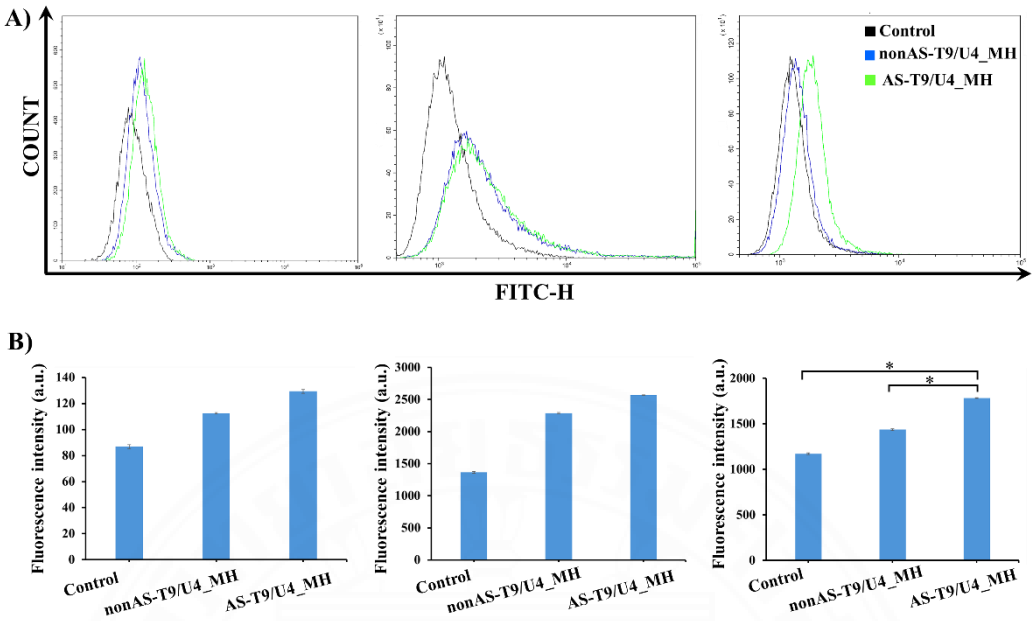

Fig. 4.4 The binding affinity of AS-T9/U4_MH was measured using flow cytometry, with the resulting histograms showing its interaction with A cells (left), B cells (middle), and C cells (right) [124].

4.2.2 Cell proliferation assay.

The cancer cells and normal colon cells were treated with MHs and cell proliferation was assessed using MTS assay. The result showed that AS-T9/U4_MH had an antiproliferation effect on C cells, but had no effect on B cell and A cells (**Fig 4.5**). Moreover, the C cells treated with AS-T9/U4_MH showed lower cell viability than those treated with nonAS-T9/U4_MH, suggesting that AS-T9/U4_MH had specific binding to cancer cells. AS-T9/U4_MH contained AS1411, the binding ligand for nucleolin receptor available on the C cells surface [127, 128]. In a study by Emilio et al., the AS1411 aptamer was shown to specifically inhibit the phosphorylation of nucleolin in HUVECs. In contrast, treatment with equivalent doses of control formulations, including a scramble sequence and ranibizumab, did not affect nucleolin phosphorylation [129]. Meanwhile, AS-T9/U4_MH had no effect on B cell and A cell, because they had low nucleolin expression. According to Dean and Kenny, the level of native nucleolin present on the plasma membrane of intestinal B cells was markedly low. This molecule was detectable using nucleolin antibody (MS-3, Santa Cruz

Biotecnology) and ab22758 (Abcam) [125]. Duncan et al. found that nucleolin was overexpressed in cancer cells compared to normal cells, including HS-27, WI-38, and MCF-10A, with normal fibroblasts showing about four times lower levels than HT-1080 and SK-MEL2 cancer cells [130].

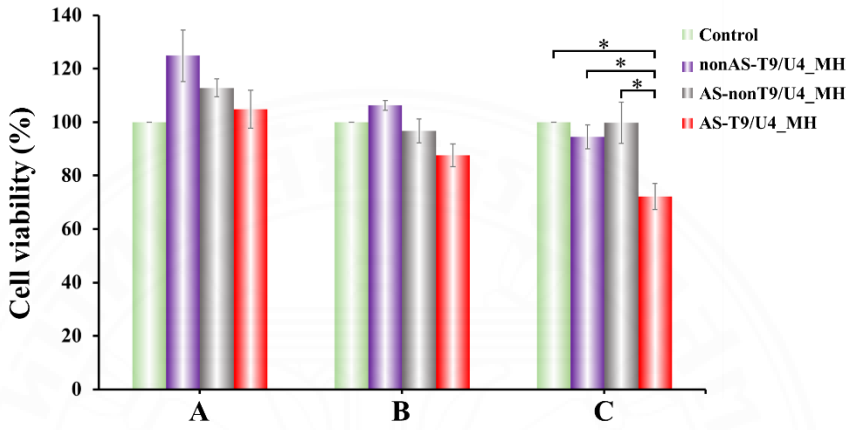

Fig. 4.5 To assess the cell viability of three cell lines—A, B, and C cells. The cells were exposed to 10 μM of nonAS-T9/U4_MH, AS-nonT9/U4_MH, and AS-T9/U4_MH, with untreated cells serving as the control for 48 h. The data represents the mean ± SD from three replicates, and statistically significant results ($P < 0.05$) relative to the control are marked with asterisks (∗) [124].

4.2.3 Intercalation of Dox into AS-T9/U4_MH.

The intercalation of Dox into AS-T9/U4_MH was evaluated via fluorescence spectroscopy, with excitation at 480 nm and emission measured at 590 nm. (**Fig. 4.6**) When Dox was mixed with the molecular hybrids, fluorescence quenching of Dox was detected suggesting Dox intercalation in double helix of DNA [102]. The efficiency of drug loading into AS-T9/U4_MH was evaluated by measuring the fluorescence intensity of Dox, which was then quantified using a calibration curve (**Fig 4.7** and **4.8)**. Our findings indicate that AS-T9/U4_MH can encapsulate nearly all of the Doxorubicin, with an encapsulation efficiency of roughly 98%. Additionally, to assess the loading capacity of AS-T9/U4_MH, by measured the fluorescence intensity of Dox. As shown in **Fig 4.9**, The results show that fluorescence intensity increases

proportionally with rising Dox concentration, indicating that the MHs have reached their maximum encapsulation capacity. Consequently, excess Dox remains in the solution. The fluorescence intensity of Dox was at its minimum detectable level when the molar ratio of AS-T9/U4_MH to Dox reached 1:1. These results indicate that our MH complex has a Dox loading capacity of one molecule per complex. To measure how much Dox was released from Dox-loaded AS-T9/U4_MH, the complex was incubated in cell culture media, collected samples at specific time points and measured their absorbance (**Fig 4.10**). The calculations were based on the maximum absorption peak at 409 nm, which is a key indicator of Dox's protonated, tautomeric state in an acidic solution [131]. After 48 hours, Doxorubicin (Dox) release from the complex was about 80%, increasing to 85% at 72 hours. The stability of the MH complex was additionally evaluated under cell culture conditions. To track the release over time, the collected solutions were analyzed using gel electrophoresis. The results from the gel electrophoresis (**Fig 4.11**) revealed a time-dependent decrease in the band intensity corresponding to the MH complex, which suggests the structural integrity of MH was compromised over the incubation period.

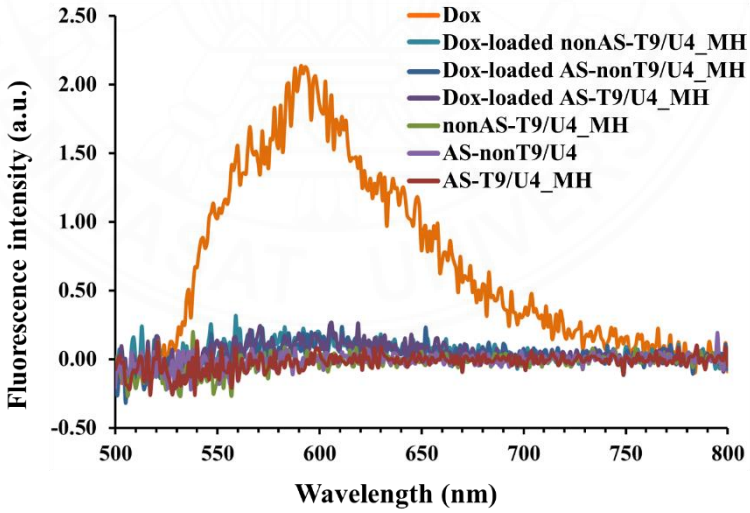

Fig. 4.6 The fluorescence spectra compare the emission of free Dox (0.95 µM) against that of several 10 µM formulations. These include Dox-loaded versions of nonAS-T9/U4_MH, AS-nonT9/U4_MH, and AS-T9/U4_MH, along with their respective drug-free counterparts [124].

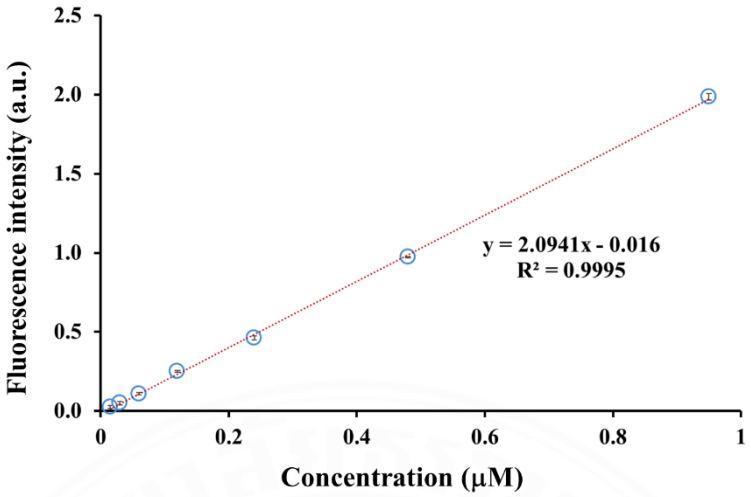

Fig 4.7 To determine the concentration of Dox remaining in the supernatant after intercalation, a standard curve was established. We prepared Dox solutions at seven different concentrations (0.95, 0.48, 0.24, 0.12, 0.06, 0.03, and 0.015 μM). The fluorescence intensity of these solutions was measured at 590 nm upon excitation at 480 nm using a fluorescence microplate reader [124].

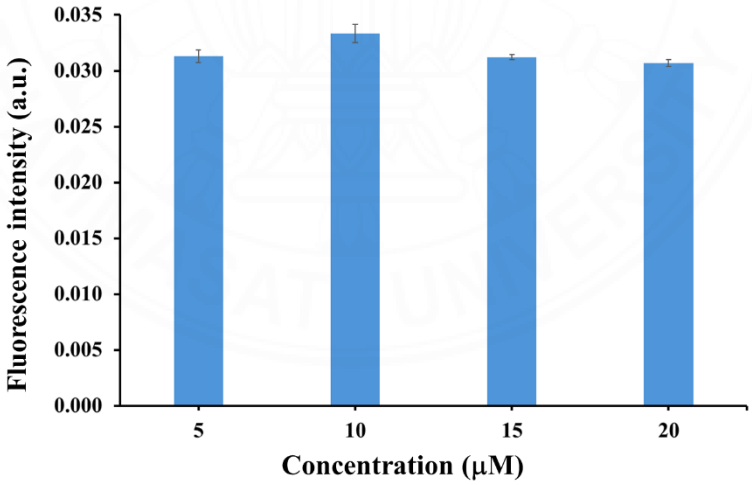

Fig 4.8 To determine the efficiency of Dox loading by preparing solutions with a constant molar ratio of 1:0.095 for AS-T9/U4_MH to Dox. The study included four concentrations for AS-T9/U4_MH (5, 10, 15, and 20 μM) and their respective Dox concentrations (0.475, 0.95, 1.9, and 3.8 μM) [124].

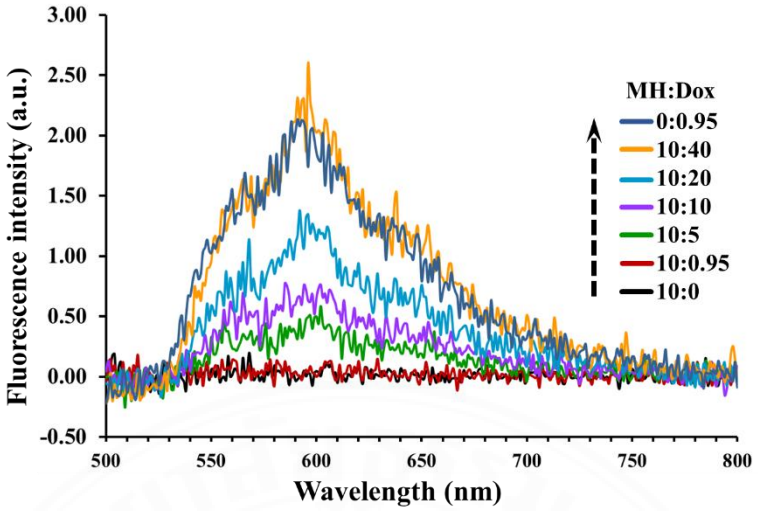

Fig 4.9 The loading capacity of AS-T9/U4_MH was assessed by incubating a 10 µM solution of the carrier with a range of Dox concentrations (0, 0.95, 5, 10, 20, and 40 µM). Following a 1.5-hour incubation period in PBS at room temperature, the Dox fluorescence intensity was quantified using a fluorescence microplate reader [124].

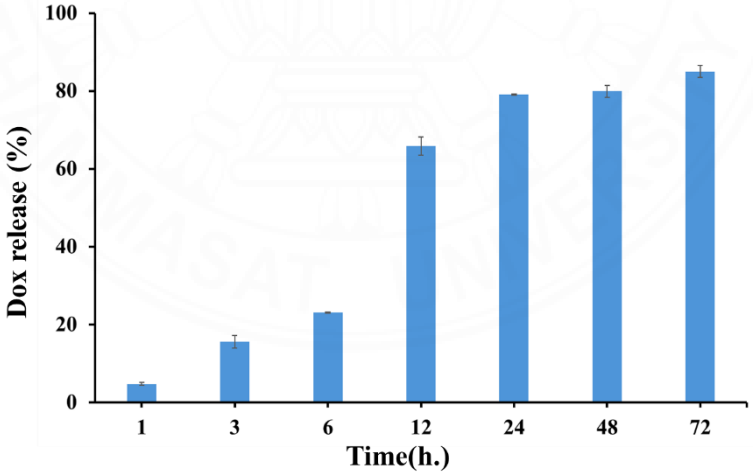

Fig 4.10 To quantify the release of Dox from Dox-loaded AS-T9/U4_MH, the compound was incubated in cell culture media at 37°C. Collected the samples at regular intervals (1, 3, 6, 12, 24, 48, and 72 hours) and measured their absorbance spectra between 350 and 800 nm. The percentage of released Dox was calculated from the absorbance value at 409 nm, with 0.95 µM of Dox serving as the 100% release reference [124].

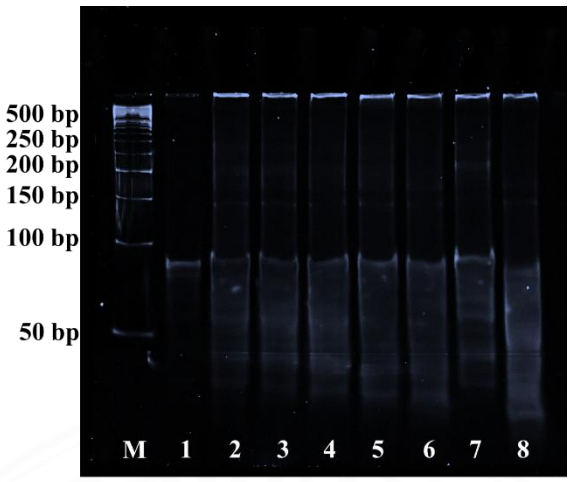

Fig 4.11 Electrophoresis was used to assess the stability of Dox-loaded AS-T9/U4_MH in cell culture media over a 72-hour period. Lane M contains a DNA marker, while Lane 1 represents the initial complex. Lanes 2 through 8 show the state of the complex at 1, 3, 6, 12, 24, 48, and 72 hours, respectively [124].

4.2.4 Effect of Dox-loaded MH on cell proliferation.

Treatment with Dox-loaded AS-T9/U4_MH resulted in lower cell viability in C cells than treatment with either Dox-loaded nonAS-T9/U4_MH or Dox-loaded AS-nonT9/U4_MH (**Fig 4.12**). When the same treatment formulations were applied to Cacao-2, and A cells, they showed no anti-proliferation on those two cells. This indicated that the integration of Dox, AS1411 aptamer and T9/U4 into a single molecular hybrid enhanced treatment effectiveness and specificity. The effectiveness of this MH was improved due to synergistic effect caused by the presence of Dox and T9/U4 ASO. Similar to a previous study, Dox intercalated in MH was less toxic than free Dox [105]. This suggested that MH strategy might provide us a way to minimize adverse effects of Dox.

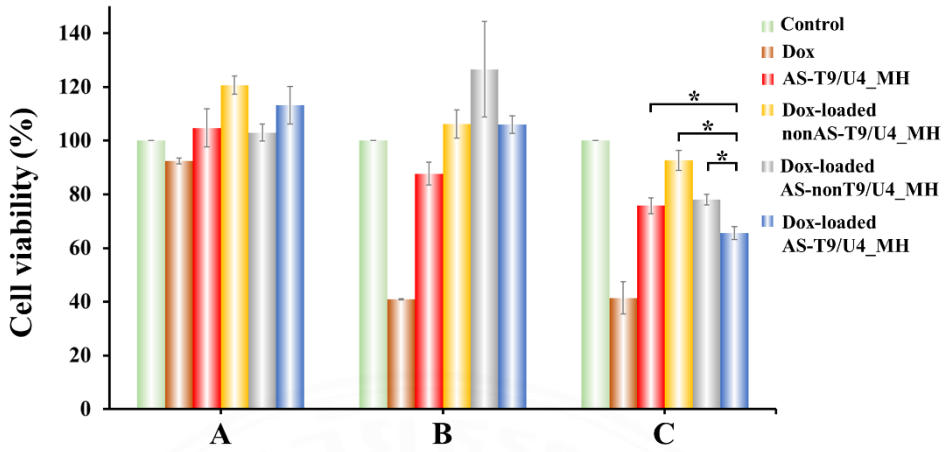

Fig. 4.12 To measure the cell viability of A, B, and C cells at 48 hours after treatment. The cells were exposed to 10 μM of Dox-loaded nonAS-T9/U4_MH, Dox-loaded AS-nonT9/U4_MH, and Dox-loaded AS-T9/U4_MH. We also tested free Dox (0.95 μM) and untreated as a control. All values represent the mean ± standard deviation (SD) from three independent experiments. Statistically significant differences are indicated by asterisks ($P < 0.05$) [124].

4.2.5 Cell apoptosis

Flow cytometry analysis revealed that treatment with AS-T9/U4_MH induced a higher rate of apoptosis in C cells than AS-nonT9/U4_MH, indicating that T9/U4 ASO suppresses C cell proliferation *in vitro* (**Fig 4.13**). In addition, Dox-loaded AS-T9/U4_MH was more effective than Dox-loaded AS-nonT9/U4_MH indicating that incorporation of Dox to MHs has significantly increased cell apoptosis indicating synergistic effect.

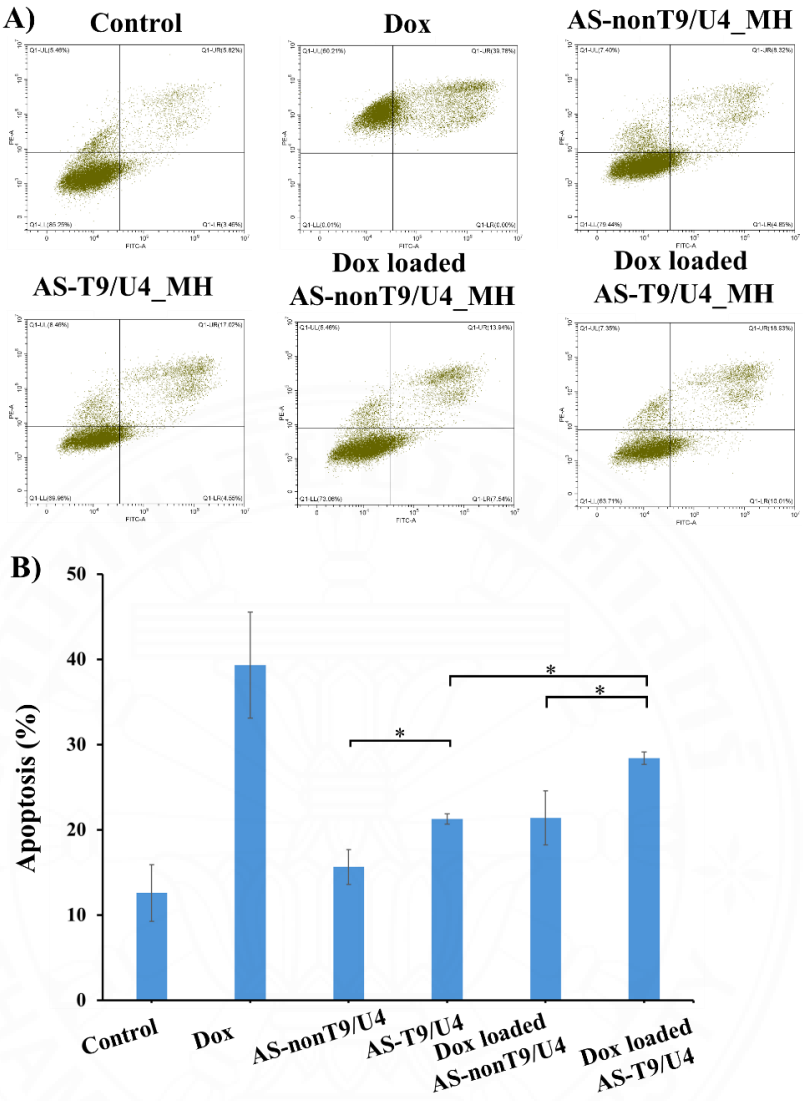

Fig. 4.13 To assess the effect of molecular hybrids on cell apoptosis, C cells were treated for 48 hours with several different compounds. The treatments included free Dox (0.95 μM), as well as four 10 μM formulations: AS-T9/U4_MH, AS-nonT9/U4_MH, Dox-loaded AS-T9/U4_MH, and Dox-loaded AS-nonT9/U4_MH. All values represent the mean ± standard deviation (SD) from three independent experiments. Statistically significant differences are indicated by asterisks ($P < 0.05$) [124].

4.2.6 Western blot analysis

To elucidate the regulation of hTERT expression by T9/U4 ASO, the protein hTERT was assessed in the C cell lines. The hTERT has been the focus of

efforts aimed at suppressing telomerase activity. It has been demonstrated that reducing hTERT levels leads to decreased cancer cell proliferation [132], enhanced apoptosis [133], and improved sensitivity to chemotherapy [134]. Both AS-nonT9/U4_MH and AS-T9/U4_MH treatments on C cells led to a significant reduction in hTERT expression levels *in vitro* (**Fig. 4.14A and 4.14B**). Similarly, cells treated with Dox-loaded AS-nonT9/U4_MH and Dox-loaded AS-T9/U4_MH exhibited significantly decreased hTERT expression (**Fig. 4.14A and 4.14B**). These results suggested that T9/U4 ASO effectively dysfunction of hTERT in C cells. Matthes et.al. demonstrated the T9/U4 modified with phosphorothioate (PS) had a potential to inhibit telomerase activity, achieving an IC_{50} = 1 nM in HL-60 cells [22]. Jackson S.R. et.al. showed that telomerase activity in A549-luC cells was reduced by over 90% when treated with a single dose of 1 μM of GRN163L [135]. Ozawa et.al. exhibited GRN163 had been effective in inhibiting telomerase activity on U-251 MG cells by 18%, 48%, and 68% at the concentration 1, 4, or 7 μM, respectively [136]. Palumbo S.L. et.al. demonstrated that G-quadruplex ligands could effectively inhibit telomerase activity. This inhibition is achieved not only by targeting telomeric G-quadruplexes but also by stabilizing the G-quadruplexes present in the hTERT promoter [137]. AS1411 aptamer belongs to the group of G-quadruplex structures. Therefore, any treatment containing the AS1411 aptamer in its composition exhibited a decrease in hTERT expression when compared to the control group (**Fig. 4.14A and 4.14B**). The hTERT expression level when treated with Dox had significantly decreased, compared to the control. Zhu et.al. demonstrated the telomerase activity on C cells was decreased when treated with Dox at 10 μM at 72 hrs [138]. Similarly, Holt et.al. treated C cells with 10 μM of Dox, it exhibited toxic effect, leading to a reduction in both telomerase activity and protein concentration [139]. Upon loading Dox into AS-T9/U4_MH, there was a significant further decrease in hTERT level compared to Dox. Collectively, these findings demonstrate that T9/U4 ASO, in combination with the AS1411 aptamer and Dox, synergistically downregulates hTERT expression.

The epithelial-mesenchymal transition (EMT) plays a critical role in cancer progression by converting epithelial cells into a mesenchymal phenotype, thereby promoting tumor development. Reports indicate that hTERT plays a role in the EMT process in CRC [140, 141]. Therefore, the level of vimentin expression was examined

since it is a protein related to the EMT process [142]. The results indicated that upon treatment with Dox, there was a slight decrease in vimentin expression in C cells compared to the control. However, this decrease was significantly notable due to the low variance observed in the data sets (**Fig. 4.14A and 4.14C**). Venkova L.S. et al. investigated the impact of vimentin on drug resistance in the MFT-16 cell line. They discovered that the mutant form of vimentin can attach to mitochondria, enhancing their membrane potential. Consequently, this alteration contributes to a decrease in the effectiveness of Dox, indicated by a shift in its concentration at IC_{50} [143]. Therefore, this explains why Dox only results in a minor decrease in the amount of vimentin. Similarly, AS1411 aptamer showed a slight decrease in vimentin in this experiment. Cho et.al. explored the therapeutic efficacy of AS1411 aptamers in SNU-761 hepatocellular carcinoma (HCC) and found that the AS1411 aptamer did not affect vimentin expression *in vitro* under both normoxic and hypoxic conditions via PI3K/Akt or ERK1/2-MAPK pathway, which are key survival signaling [144]. Comparison between nonT9/U4 and T9/U4 ASO targeting hTERT revealed a significant decrease in vimentin expression levels in C cells treated with AS-nonT9/U4_MH and AS-T9/U4_MH, corresponding to cells treated with Dox-loaded AS-nonT9/U4_MH and Dox-loaded AS-T9/U4_MH. These results suggest that T9/U4 ASO effectively reduces vimentin levels via hTERT dysfunction.

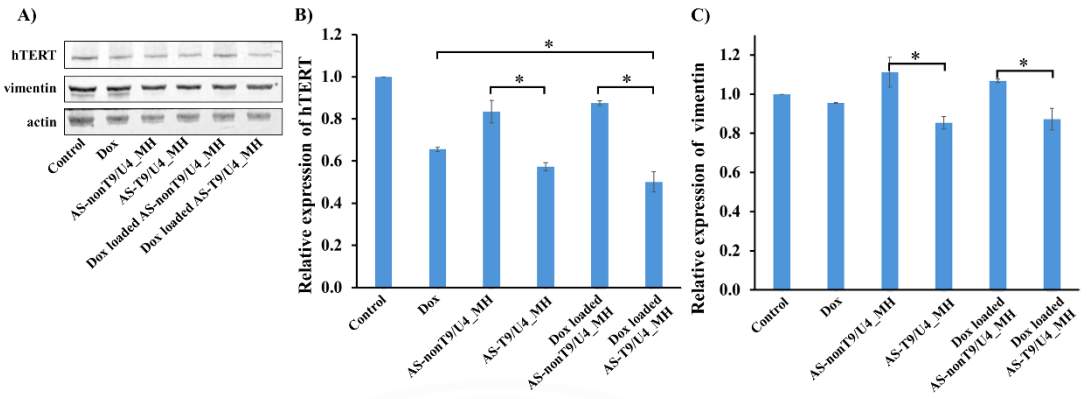

Fig. 4.14 (A) The expression of hTERT and vimentin in C cells was measured after a 48-hour treatment with 0.95 µM of Dox and 10 µM of various formulations: AS-T9/U4_MH, AS-nonT9/U4_MH, Dox-loaded AS-T9/U4_MH, and Dox-loaded AS-nonT9/U4_MH. Western blot analysis was used to determine the relative expression of (B) hTERT and (C) vimentin through densitometric analysis. All values represent the mean ± standard deviation (SD) from three independent experiments. Statistically significant differences are indicated by asterisks ($P < 0.05$) [124].

The pathway of apoptosis stands out as the most extensively studied programmed cell death pathway. It is associated with multiple pathways. Dox can stimulate the intrinsic apoptosis pathway by inducing the activation and translocation of Bax/Bak from the cytosol to the outer membrane of mitochondria. This action leads to the permeabilization of the mitochondrial outer membrane, facilitating the release of various proteins into the cytoplasm [145]. Another key characteristic of AS1411, a specific binding to nucleolin, which consequently inhibits the proliferation and induces cancer cell death. Due to AS1411 inhibiting DNA replication, which is typically suppressed by nucleolin [16, 17, 146]. Within apoptotic pathways, Bcl-2 and Bax are significant proteins. Bcl-2 inhibits apoptosis, while Bax promotes apoptotic cell death. Therefore, the expression level of Bax and Bcl-2 were evaluated within this pathway that it leads to upregulation of Bax, consequently leading to decreased expression of the antiapoptotic protein Bcl-2 [147]. This experiment AS-nonT9/U4_MH, AS-T9/U4_MH, Dox-loaded AS-nonT9/U4_MH and Dox-loaded AS-T9/U4_MH were

treated on C cells. Comparing AS-nonT9/U4_MH with Dox-loaded AS-nonT9/U4_MH, and AS-T9/U4_MH with Dox-loaded AS-T9/U4_MH, Bcl-2 levels were significantly reduced, while Bax levels were significantly elevated (**Fig. 4.15A, 4.15B, and 4.15C**). These results suggested a notable impact not only with AS1411 but also with the addition of Dox, demonstrating a synergistic effect. Sharifi et. al. demonstrated that treating MCF-7 breast cancer cells with Dox induced apoptosis through the mitochondrial pathway by decreasing the expression levels of the anti-apoptotic protein Bcl-x_L and increasing the expression levels of the pro-apoptotic protein Bax. This led to a significant increase in the Bax/Bcl-x_L ratio across all doses [148]. Pilco-Ferreto et al. found that Dox triggered apoptosis in MCF-10F, MCF-7, and MDA-MB-231 cells through increased expression of Bax, caspase-8, and caspase-3, along with decreased Bcl-2 levels [149]. Besides, Dox could integrate with different nanocarriers such as metal nanoparticles [150], DNA nanostructures [151], and mesoporous silica nanoparticles [152]. Consequently, Dox has found extensive application in chemotherapy. Here, AS1411 aptamer emerges as a promising target molecule to combine with Dox, thereby enhancing the synergistic effect. Cheng et al. reported that AS1411 induces apoptosis and arrests the cell cycle in human glioma cells, while reducing cell viability via upregulation of p53 and downregulation of Bcl-2 and Akt1 [153]. In culture, the T9/U4 modified structure experienced telomere shortening, leading to either cellular senescence or apoptosis after a duration typically corresponding with the initial telomere length [154]. Thus, the result of C cells treated with AS-nonT9/U4_MH and AS-T9/U4_MH showed a significant decrease in Bcl-2 and an increase in Bax, suggesting that T9/U4 ASO effectiveness in increasing cell apoptosis. Similarly, cells treated with Dox-loaded AS-nonT9/U4_MH and Dox-loaded AS-T9/U4_MH exhibited greater efficacy compared to the complex without Dox-loading, indicating a synergistic interaction between them [155].

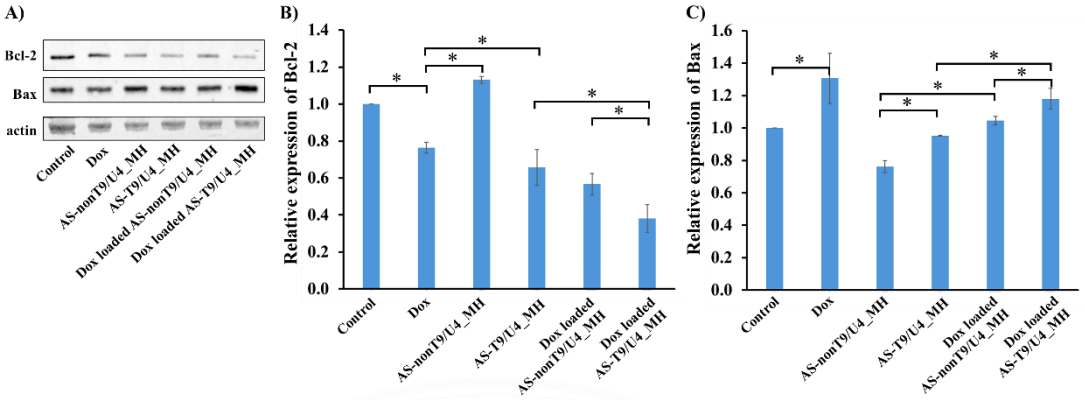

Fig. 4.15 To investigate effect of molecular hybrid on apoptosis. (A). The expression of the pro- and anti-apoptotic proteins Bax and Bcl-2 were analyzed in C cells. The cells were treated for 48 hours with 0.95 µM of Dox and 10 µM of AS-T9/U4_MH, AS-nonT9/U4_MH, Dox-loaded AS-T9/U4_MH, and Dox-loaded AS-nonT9/U4_MH. Densitometric analysis of the Western blot shows the relative expression levels of (B) Bcl-2 and (C) Bax for each condition. All values represent the mean ± standard deviation (SD) from three independent experiments. Statistically significant differences are indicated by asterisks ($P < 0.05$) [124].

4.3 Activity of aptamer train (AT)

4.3.1 Stability and binding of AT *in vitro*.

The specific binding capability of the polyvalent AS1411 aptamer was evaluated using confocal laser scanning microscopy (CLSM) on A, B, and C cell lines. Fluorescence imaging revealed that the FAM-labeled AT exhibited selective affinity toward C cells, which can be attributed to the elevated levels of nucleolin—a protein commonly overexpressed in cancer cells [156, 157] (**Fig 4.16**). Conversely, B cell and A cells exhibited weaker fluorescence signals, suggesting reduced binding of the FAM-labeled AT. This difference is likely due to the lower levels of nucleolin expression in these cell types [125, 130].

To confirm this finding, the fluorescence intensity of binding between AS1411 aptamer with nucleolin was determined using flow cytometry. The

results showed that C cell exhibited notably stronger fluorescence intensity upon binding with FAM-labeled AT, which is attributed to the higher quantity of AS1411 aptamers present in the polyvalent AT (**Fig. 4.17**). In contrast, B cell and A cells showed low fluorescence signals, indicating a limited presence of nucleolin on their surfaces. These findings strongly support the selective binding and internalization of AT with polyvalent AS1411 aptamers by C cells over B cell and A cells. These observations align with the microscopy assay results, further confirming the specific targeting of the C cell line by the polyvalent system.

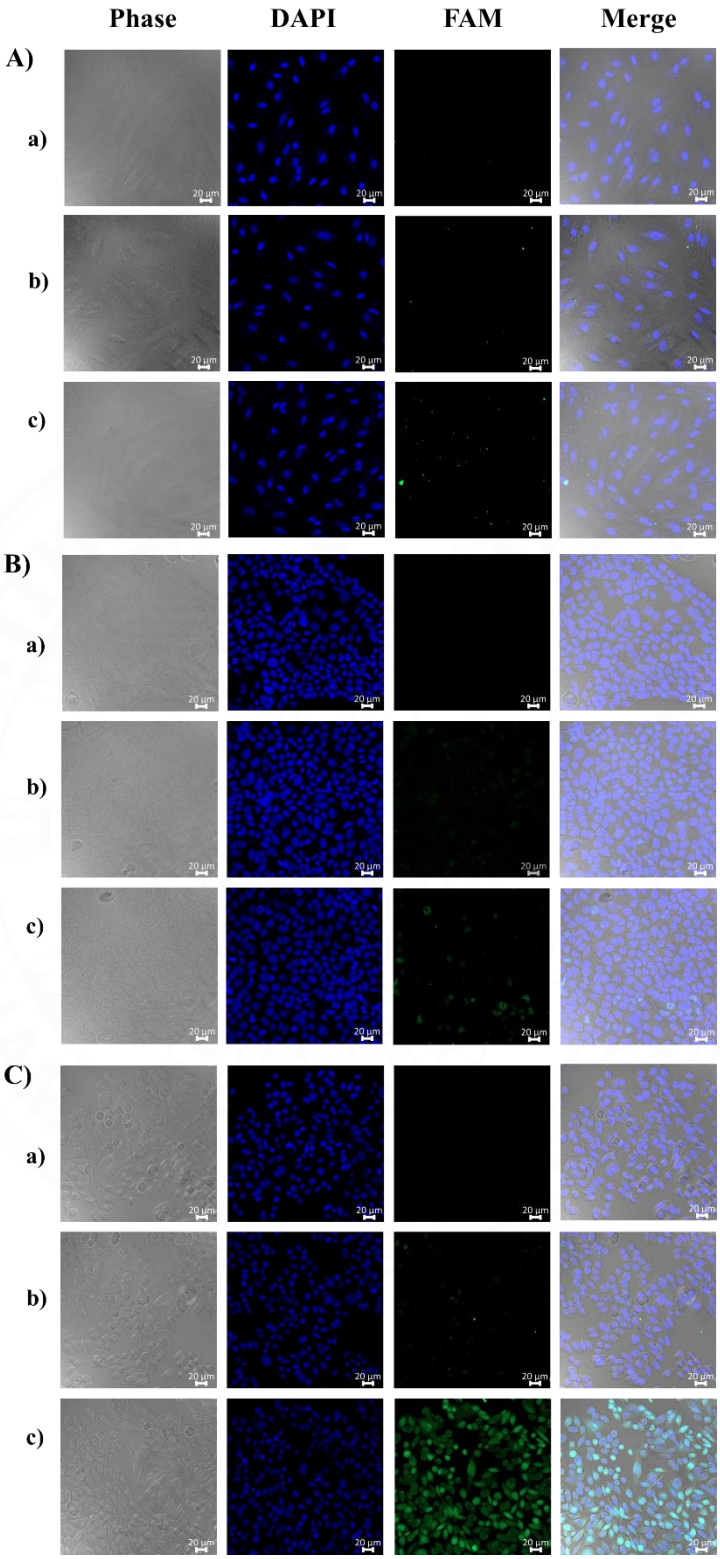

Fig. 4.16 Fluorescence image used to visualize the uptake of (b) FAM-labeled CT and (c) FAM-labeled AT in three cell lines: (A) A cells, (B) B cells, and (C) C cells. Untreated used as a control shown in (a) for comparison.

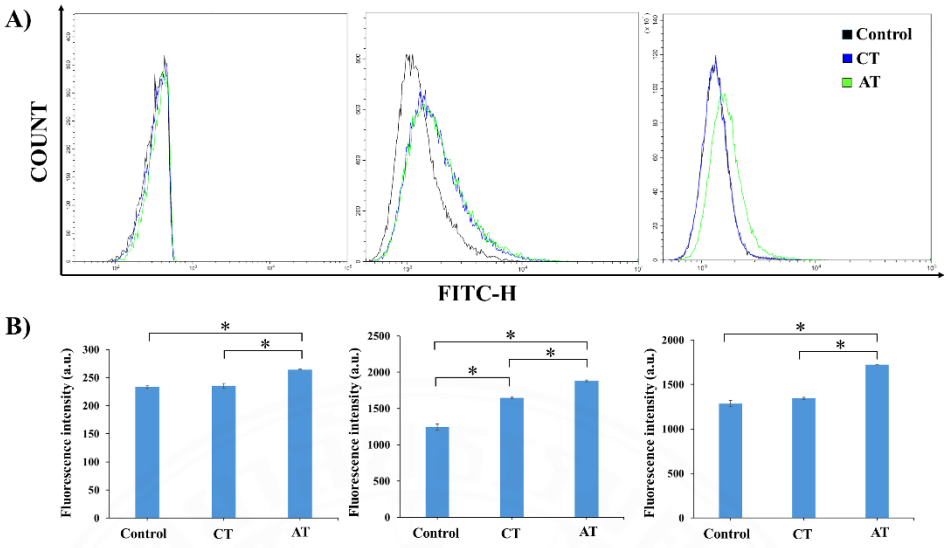

Fig. 4.17 Flow cytometry used to quantify the AT binding to three different cells line: A, B, and C cells, as depicted in the histogram from left to right, respectively.

4.3.2 Cytotoxicity assay of MTZ.

To evaluate the cytotoxic effects of MTZ on cancer cell proliferation, B and C cells were exposed to varying concentrations of MTZ. The results indicated that MTZ induced cytotoxicity in B and C cells in a dose-dependent which is IC_{50} value on B and C cells were 0.15 and 0.09 µM, respectively (**Fig 4.18**). The values obtained were later applied in subsequent experiments, including AT intercalation, cell proliferation, apoptosis assay, and Western blot analysis.

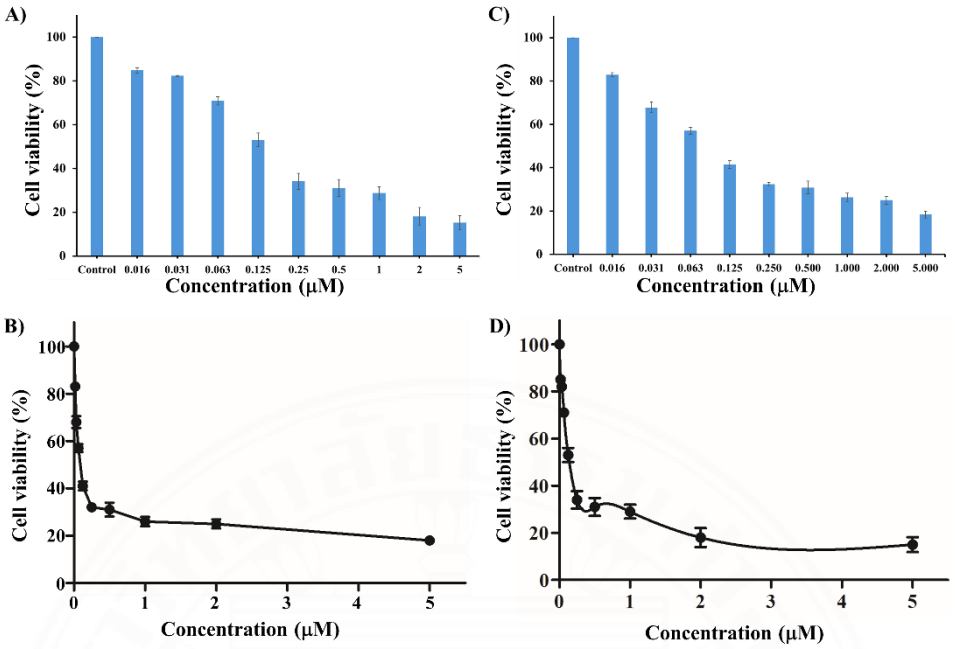

Fig. 4.18 To quantify IC_{50} value of MTZ for B and C cells. The percentage of cell viability was observed after 48 h. of treatment. (A, B) C cells and (C, D) B cells were exposed to MTZ at 0.016, 0.031, 0.063, 0.125, 0.25, 0.5, 1.0, 2.0, 5.0 μM, and no treatment as a control.

4.3.3 Intercalation of MTZ into AT.

MTZ exerts its therapeutic effects mainly by intercalating into DNA, which interferes with vital cellular functions in rapidly proliferating cells. Nonetheless, this mechanism also causes considerable toxicity in healthy tissues, resulting in side effects like myelosuppression [158]. Embedding MTZ within a DNA duplex has been identified as a promising approach to minimize its cytotoxic effects. Fluorescence spectroscopy using a microplate reader was employed to assess the incorporation of MTZ into AT. Literature indicates that MTZ exhibits fluorescence with excitation at 610 nm and peak emission at 685 nm [114, 123]. The fluorescence intensity diminished upon mixing MTZ with AT and was entirely quenched when the molar ratio of MTZ to AT reached 0.09:1 (**Fig. 4.19**). Furthermore, the loading efficiency (LE) of AT, determined using equation (1), was 93% for MTZ-loaded CT and 96% for MTZ-loaded AT.

$$LE = \left(\frac{FL_i - FL_r}{FL_i} \; x \; 100\right) \quad (1)$$

where FL_i is an initial MTZ fluorescence intensity

FL_r is a remaining MTZ fluorescence intensity after intercalation

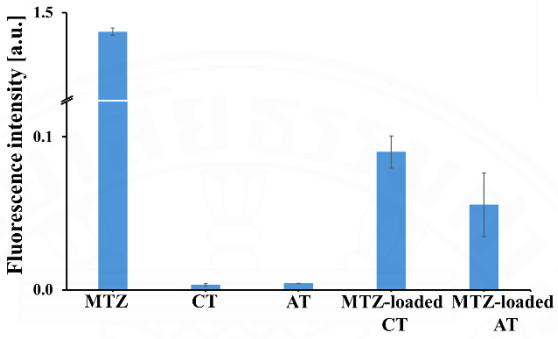

Fig. 4.19 The fluorescence was used to compare the emission of 0.09 µM of free MTZ to that of the various complexes. The complexes, all at a concentration of 1 µM, included the empty carriers (CT and AT) and the drug-loaded formulations (MTZ-loaded CT and MTZ-loaded AT).

4.3.4 MTZ loading capacity into AT.

To assess the loading capacity, different concentrations of MTZ were incubated with AT, and the fluorescence signal of MTZ was measured. The drug loading capacity (LC) was determined according to equation (2). **Fig. 4.20** illustrates that at an AT to MTZ molar ratio of 1:5, the MTZ loading capacity decreased to 91%, and at a ratio of 1:10, it declined sharply to 68%. These findings indicated that a single AT molecule can encapsulate up to five MTZ molecules.

$$LC = \left(\frac{FL_{MTZ} - FL_{AT}}{FL_{MTZ}} \; x \; 100\right) \quad (2)$$

where FL_{MTZ} is fluorescence intensity of MTZ at 0.09 µM

FL_{AT} is fluorescence intensity of MTZ incorporated AT

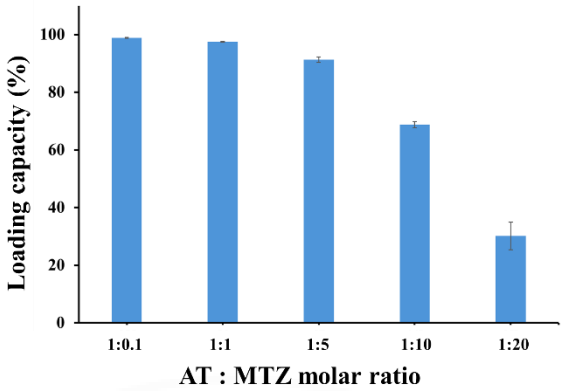

Fig. 4.20 Loading capacity of MTZ incorporated into AT at various molar ratios.

4.3.5 MTZ released.

To assess MTZ release, MTZ-loaded AT was incubated in cell culture media at specific time points, and the media were collected to measure absorbance, evaluating the carrier potential of AT (**Fig 4.21A**). The absorption spectra demonstrated a time-dependent increase in MTZ absorbance, indicating progressive release over the incubation period. The percentage of drug released was determined by measuring the maximum absorbance at 610 nm, corresponding to the characteristic peak of MTZ. Cumulative MTZ release from the complex reached 81 % at 48 hours and increased to 85 % at 72 hours (**Fig 4.21B**).

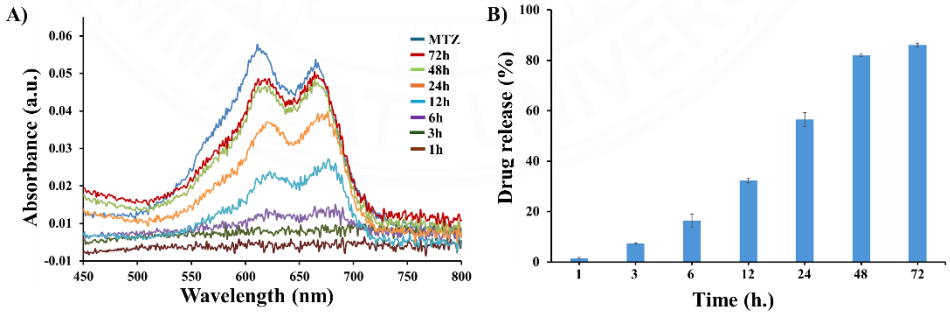

Fig. 4.21 (A) The absorption spectra of MTZ released from MTZ-loaded AT were recorded following incubation in cell culture media at predetermined time intervals. (B) MTZ release was quantified based on the maximum absorption peak at 610 nm, with absorbance values normalized to a reference concentration of 0.09 µM MTZ.

Moreover, AT stability is essential for its effective application in cell culture systems. AT stability was assessed by analyzing release medium samples collected at predetermined time points using gel electrophoresis. Analysis of the gel image indicated a progressive reduction in the AT band intensity over time (**Fig. 4.22**). Notably, AT showed nearly complete degradation at the 48-hour mark, this incubation time was used for the following cell proliferation assay.

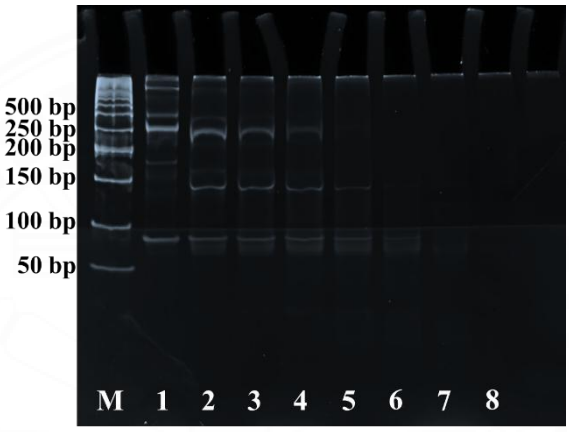

Fig. 4.22 Gel electrophoresis analysis of the released solution collected at specific time points. Lane M represents the DNA marker, lane 1 corresponds to MTZ-loaded AT, and lanes 2 through 8 represent sampling times at 1, 3, 6, 12, 24, 48, and 72 hours, respectively.

4.3.6 Effect of MTZ-loaded AT on cell proliferation.

The effect of free MTZ on cell viability was evaluated in B cell and C cell cancer cell lines, as well as in non-cancerous A cell colon cells. The findings showed that free MTZ was toxic to B and C cells cancer cells but had no notable impact on A cell normal colon cells, indicating its potential as a suitable anticancer agent for colorectal cancer therapy (**Fig 4.23**)**.** MTZ-loaded AT treatment resulted in a significantly lower cell viability in B cells compared to treatment with MTZ-loaded CT. Nevertheless, cell viability remained above 70% for both formulations, suggesting that the molecular train had limited antiproliferative effectiveness on B cells, likely because of inadequate nucleolin expression on the cell surface [125, 126]**.** In C cells, treatment with MTZ-loaded AT resulted in significantly reduced cell viability

compared to CT, suggesting that the AS1411 aptamer contributed to the inhibition of cell proliferation**.** The internalization of AS1411-nucleolin complexes occurs via clathrin-dependent endocytosis and macropinocytosis pathway after binding. After internalization, AS1411 builds up in the cytoplasm and nucleoli, disrupting the role of nucleolins in mRNA stability and ribosome synthesis. Downstream consequences of this disturbance include decreased cancer cell growth and the triggering of apoptosis [17]**.** Additionally, MTZ-loaded AT significantly reduced cell growth when compared to both MTZ-loaded CT and free MTZ. These findings suggest that more efficient drug administration was achieved by the polyvalent AS1411 aptamer, improving specific binding to nucleolin which is overexpressed on the surface of C cells**.** The polyvalent AS1411 aptamer system decreases the cytotoxicity of the anticancer medication, acting as a possible drug carrier by intercalation. Toxicity of MTZ was decreased when it was intercalated into double-stranded DNA in all examined cell lines, including A, B, and C cell.

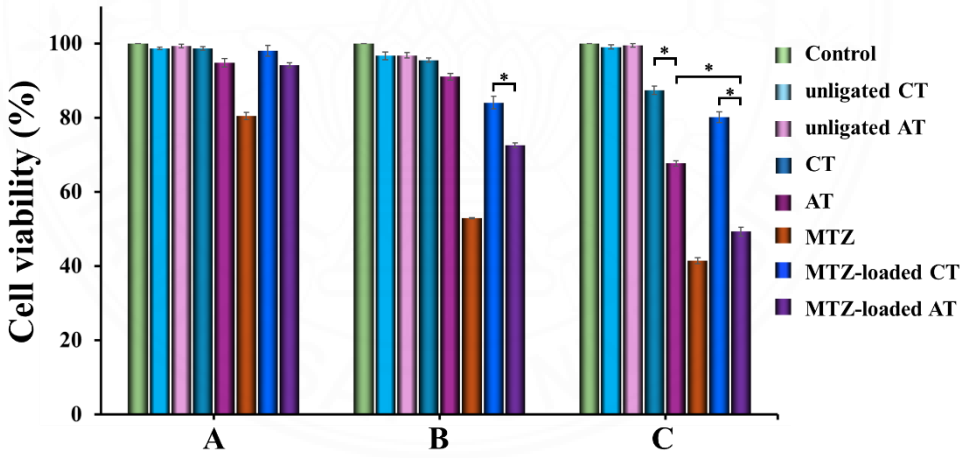

Fig. 4.23 To determine the cytotoxic effects of AT: A, B, and C cells were incubated for 48 hours. The treatments included 0.09 µM of free MTZ, control with no treatment, and several 1 µM formulations: the unligated complexes (unligated CT, unligated AT), the fully ligated complexes (CT, AT), and their MTZ-loaded counterparts (MTZ-loaded CT, MTZ-loaded AT). All values represent the mean ± standard deviation (SD) from three independent experiments. Statistically significant differences are indicated by asterisks ($P < 0.05$).

4.3.7 Effect of MTZ-loaded AT on cell apoptosis.

To access cell apoptosis C cells were treated with 0.09 μM of MTZ, 1 μM of unligated CT, unligated AT, CT, AT, MTZ-loaded CT, MTZ-loaded AT, and no treatment as a control and characterized using flow cytometry. The result of the cells treated with the group of complexes without MTZ showed that AT had significantly increased the percentage of cell apoptosis more than unligated CT, unligated AT, and CT. This result verified that AT successfully suppressed the proliferation of C cells in vitro (**Fig. 4.24A** and **4.24B**). AS1411 binds to nucleolin, impairing its normal functions, which in turn destabilizes Bcl-2 mRNA, a key anti-apoptotic protein that disrupts cellular homeostasis, and ultimately triggers cell cycle arrest and apoptosis [146, 159]. Furthermore, integrating MTZ into AT significantly amplified its pro-apoptotic effect compared to MTZ-loaded CT [160]. Enhanced effectiveness underscores the potential of AT, the multivalent AS1411, as a promising delivery platform for therapeutic agents such as MTZ, offering a viable strategy for improved cancer treatment.

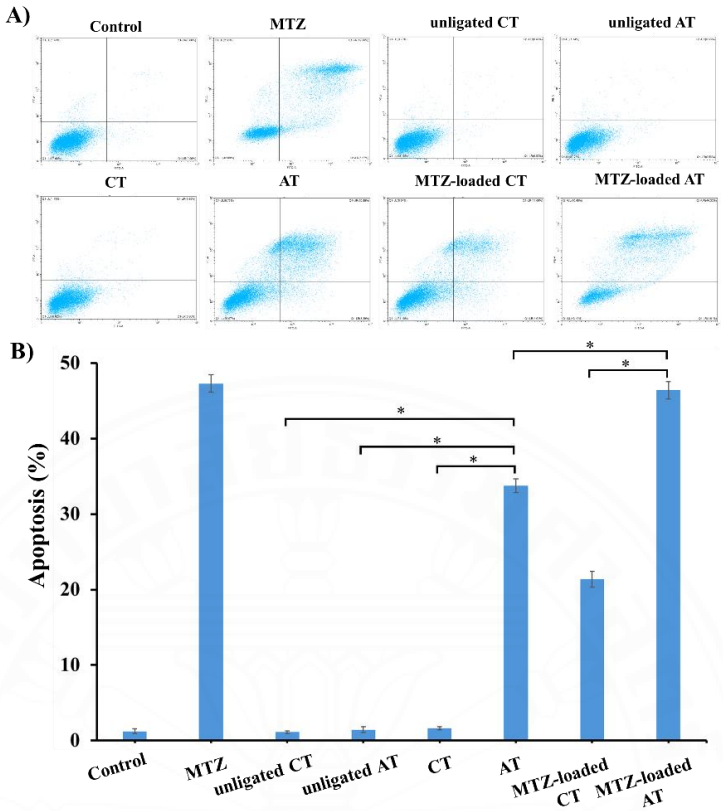

Fig. 4.24 To evaluate the effect of various formulations on apoptosis, C cells were treated for 48 hours. The treatments included 0.09 μM of MTZ, untreated cells as a control, and several 1 μM formulations: unligated CT and AT, ligated CT and AT, and their respective drug-loaded versions. The resulting (A) flow cytometry plots and (B) quantitative apoptosis counts are presented. All values represent the mean ± standard deviation (SD) from three independent experiments. Statistically significant differences are indicated by asterisks ($P < 0.05$).

4.3.8 Effect of MTZ-loaded AT on PI3K/Akt pathway.

The PI3K/Akt signaling pathway plays a vital role in controlling key cellular functions such as growth, proliferation, survival, and metabolism. Activated Akt then modulates several downstream targets that support cell survival and growth [161]. Aberrant regulation of this pathway is linked to a wide range of diseases, most notably cancer. C cells were treated to assess the effect of MTZ on the PI3K/Akt

signaling pathway. The results demonstrated that MTZ treated cells had a marked decrease in Akt expression (**Fig 4.25A** and **4.25B**).

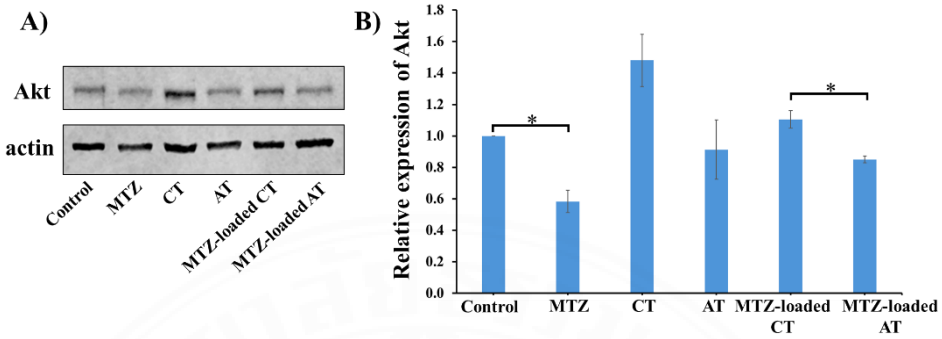

Fig. 4.25 To assess the effect of AT on Akt expression, a Western blot was performed on C cells. The treatments included 0.09 μM of MTZ, 1 μM of the empty complexes CT and AT, their drug-loaded versions (MTZ-loaded CT and MTZ-loaded AT), and an untreated as a control. (A) The Western blotting image and (B) the quantified expression levels are presented. All values represent the mean ± standard deviation (SD) from three independent experiments. Statistically significant differences are indicated by asterisks ($P < 0.05$).

4.3.9 Effect of MTZ-loaded AT on apoptosis pathway.

Members of the Bcl-2 protein family govern intrinsic apoptosis by either supporting cell survival or triggering programmed cell death. Among the Bcl-2 family members, Bcl-2 itself acts as an anti-apoptotic regulator by inhibiting caspase activation and thereby blocking the progression of apoptosis. In contrast, Bax functions as a pro-apoptotic protein by promoting mitochondrial outer membrane permeabilization, which facilitates the release of cytochrome c and triggers activation of the caspase cascade. The balance between Bcl-2 and Bax expression is crucial in determining cell fate; an elevated Bcl-2/Bax ratio supports cell survival, whereas a reduced ratio increases susceptibility to apoptosis [162]. Therapeutic approaches targeting the modulation of the Bcl-2/Bax ratio are under investigation to promote apoptosis in cancer cells. Experiments were performed in C cells to investigate the effect of MTZ

on Bcl-2 and Bax, critical components of the intrinsic apoptosis pathway. MTZ treatment resulted in a significant decrease in the Bcl-2/Bax ratio compared to untreated controls (**Fig. 4.26A and 4.26B**). Corresponding analyses revealed downregulation of Bcl-2 and upregulation of Bax (**Fig. 4.26C and 4.26D**), suggesting that MTZ promotes apoptosis and inhibits cell proliferation. Likewise, AT also exhibited a markedly reduced Bcl-2/Bax ratio (**Fig. 4.26A** and **4.26B**), reinforcing its anti-proliferative potential. These findings suggest that AT improves binding site accessibility and promotes cellular internalization. Incorporation of MTZ into the AT complex led to a significantly reduced Bcl-2/Bax ratio (**Fig. 4.26A** and **4.26B**), indicating a synergistic enhancement of pro-apoptotic activity.

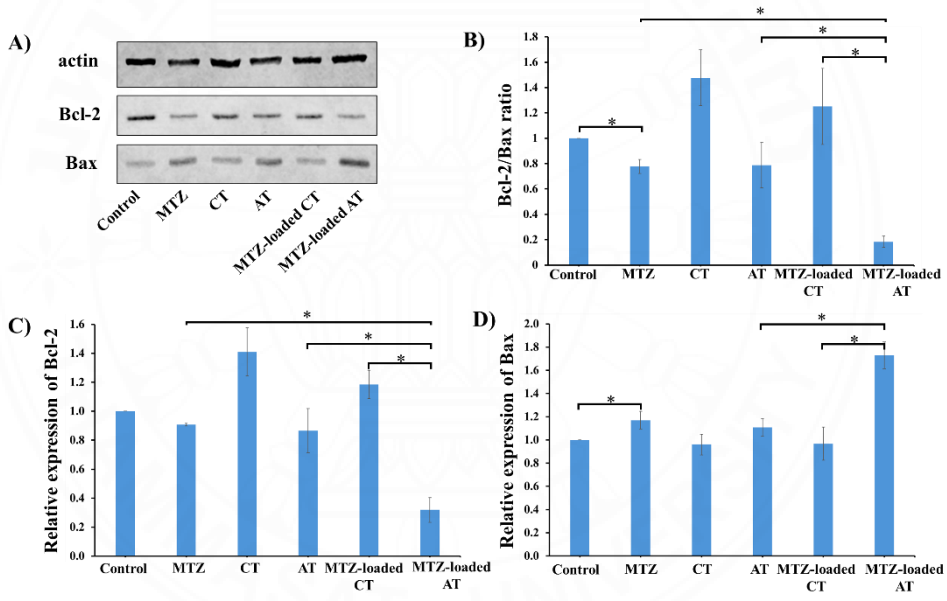

Fig. 4.26 To assess the balance of anti- and pro-apoptotic proteins, a Western blot was performed on C cells. The cells were exposed to 0.09 μM of MTZ, 1 μM of the empty carriers (CT, AT), their drug-loaded versions (MTZ-loaded CT, MTZ-loaded AT), and were also left untreated as a control. The analysis of the blots provides (A) Western blotting image and the relative expression of the (B) Bcl-2/Bax ratio, (C) Bcl-2, and (D) Bax. All values represent the mean ± standard deviation (SD) from three independent experiments. Statistically significant differences are indicated by asterisks ($P < 0.05$).

CHAPTER 5
CONCLUSION

5.1 Conclusion

Cancer is the leading cause of death which has a significant effect on public healthcare management. Most patients suffer from side effects of therapeutic drugs, partly causing by a lack of specificity. To improve drug specificity and further enhance the effectiveness of therapeutic agents, MHs composed of aptamer, ASO, and anticancer drug were proposed. The MHs were formed via oligonucleotide base pairing and enzymatic ligation. Research activities were as follows: i) AS-T9/U4_MH was prepared via oligonucleotide hybridization ii) aptamer train (AT) was formed through hybridization and ligation reaction, iii) doxorubicin was loaded to AS-T9/U4_MH, and mitoxantrone was loaded to AT, and iv) the molecular hybrid was evaluated for its effect on cell proliferation and biomolecular pathway.

The formation of MH was verified by gel electrophoresis indicating success in preparation of AS – T9/U4_MH and AT. AS–T9/U4_MH and AT exhibited specificity toward C cells, with negligible activity on B cells and A cells. This cell-type selectivity was confirmed through cell viability assays, fluorescence microscopy, and flow cytometry analysis. Moreover, AS–T9/U4_MH functioned as a carrier for the co-delivery of ASO and Dox, with cell viability assays revealing a synergistic effect between the two agents. The intercalation of Dox into the DNA double helix reduced its cytotoxic effect. Notably, treatment with Dox-loaded AS-T9/U4_MH significantly lowered the expression of hTERT and vimentin in C cells, highlighting its capacity to impede epithelial-mesenchymal transition (EMT) and tumor progression. Finally, the influence of MHs on apoptotic signaling pathways was examined, showing a marked downregulation of Bcl-2 and an upregulation of Bax in C cells following treatment with Dox-loaded AS-T9/U4_MH. These findings imply that apoptosis is mediated via the mitochondrial pathway, with a synergistic interaction between Dox and the T9/U4 antisense oligonucleotide contributing to the observed effect.

Regarding AT activity, the polyvalent AS1411 aptamer demonstrated up to a tenfold increase in binding affinity compared to its monovalent counterpart, particularly when evaluated against AS-T9/U4_MH. Cell viability assays indicated that AT efficiently delivered MTZ to target cells while simultaneously mitigating its cytotoxic effect. MTZ-loaded AT also influenced cell proliferation signaling pathways, notably PI3K/Akt and apoptosis, by downregulating the expression of Akt and Bcl-2 while upregulating Bax in C cells.

The success of these studies underscores the high specificity and low toxicity of our drug delivery system, highlighting its potential as a platform for the drug delivery of other cancer therapeutics.

REFERENCES

1. Arruebo M, Vilaboa N, Sáez-Gutierrez B, Lambea J, Tres A, Valladares M, et al. Assessment of the evolution of cancer treatment therapies. Cancers (Basel). 2011;3(3):3279-330.

2. Schirrmacher V. From chemotherapy to biological therapy: A review of novel concepts to reduce the side effects of systemic cancer treatment (Review). Int J Oncol. 2019;54(2):407-19.

3. Hosseini A, Sahebkar A. Reversal of Doxorubicin-induced Cardiotoxicity by Using Phytotherapy: A Review. J Pharmacopuncture. 2017;20(4):243-56.

4. Lefrak EA, Piťha J, Rosenheim S, Gottlieb JA. A clinicopathologic analysis of adriamycin cardiotoxicity. Cancer. 1973;32(2):302-14.

5. Swain SM, Whaley FS, Ewer MS. Congestive heart failure in patients treated with doxorubicin. Cancer. 2003;97(11):2869-79.

6. Feitelson MA, Arzumanyan A, Kulathinal RJ, Blain SW, Holcombe RF, Mahajna J, et al. Sustained proliferation in cancer: Mechanisms and novel therapeutic targets. Semin Cancer Biol. 2015;35 Suppl(Suppl):S25-s54.

7. Leal-Esteban LC, Fajas L. Cell cycle regulators in cancer cell metabolism. Biochimica et Biophysica Acta (BBA) - Molecular Basis of Disease. 2020;1866(5):165715.

8. Hubbell JA, Langer R. Translating materials design to the clinic. Nat Mater. 2013;12(11):963-6.

9. Zhang XQ, Xu X, Bertrand N, Pridgen E, Swami A, Farokhzad OC. Interactions of nanomaterials and biological systems: Implications to personalized nanomedicine. Adv Drug Deliv Rev. 2012;64(13):1363-84.

10. Sim S, Wong NK. Nanotechnology and its use in imaging and drug delivery (Review). Biomed Rep. 2021;14(5):42.

11. Wu X, Chen J, Wu M, Zhao JX. Aptamers: active targeting ligands for cancer diagnosis and therapy. Theranostics. 2015;5(4):322-44.

12. Ruscito A, DeRosa MC. Small-Molecule Binding Aptamers: Selection Strategies, Characterization, and Applications. Frontiers in Chemistry. 2016;4.

13. Fadeev M, O'Hagan MP, Biniuri Y, Willner I. Aptamer–Protein Structures Guide In Silico and Experimental Discovery of Aptamer–Short Peptide Recognition Complexes or Aptamer–Amino Acid Cluster Complexes. The Journal of Physical Chemistry B. 2022;126(44):8931-9.

14. Cerchia L, Giangrande PH, McNamara JO, de Franciscis V. Cell-specific aptamers for targeted therapies. Methods Mol Biol. 2009;535:59-78.

15. Berger CM, Gaume X, Bouvet P. The roles of nucleolin subcellular localization in cancer. Biochimie. 2015;113:78-85.

16. Bates PJ, Laber DA, Miller DM, Thomas SD, Trent JO. Discovery and development of the G-rich oligonucleotide AS1411 as a novel treatment for cancer. Experimental and Molecular Pathology. 2009;86(3):151-64.

17. Bates PJ, Reyes-Reyes EM, Malik MT, Murphy EM, O'Toole MG, Trent JO. G-quadruplex oligonucleotide AS1411 as a cancer-targeting agent: Uses and mechanisms. Biochimica et Biophysica Acta (BBA) - General Subjects. 2017;1861(5, Part B):1414-28.

18. Ashrafuzzaman M. Aptamers as both drugs and drug-carriers. Biomed Res Int. 2014;2014:697923.

19. Kim D-H, Seo J-M, Shin K-J, Yang S-G. Design and clinical developments of aptamer-drug conjugates for targeted cancer therapy. Biomaterials Research. 2021;25(1):42.

20. Giudice V, Mensitieri F, Izzo V, Filippelli A, Selleri C. Aptamers and Antisense Oligonucleotides for Diagnosis and Treatment of Hematological Diseases. Int J Mol Sci. 2020;21(9).

21. Montaño-Samaniego M, Bravo-Estupiñan DM, Méndez-Guerrero O, Alarcón-Hernández E, Ibáñez-Hernández M. Strategies for Targeting Gene Therapy in Cancer Cells With Tumor-Specific Promoters. Frontiers in Oncology. 2020;10.

22. Matthes E, Lehmann C. Telomerase protein rather than its RNA is the target of phosphorothioate-modified oligonucleotides. Nucleic Acids Res. 1999;27(4):1152-8.

23. Seeman NC. Nucleic acid junctions and lattices. Journal of Theoretical Biology. 1982;99(2):237-47.

24. LaBean TH, Yan H, Kopatsch J, Liu F, Winfree E, Reif JH, et al. Construction, Analysis, Ligation, and Self-Assembly of DNA Triple Crossover Complexes. Journal of the American Chemical Society. 2000;122(9):1848-60.

25. Zhang C, Ko SH, Su M, Leng Y, Ribbe AE, Jiang W, et al. Symmetry Controls the Face Geometry of DNA Polyhedra. Journal of the American Chemical Society. 2009;131(4):1413-5.

26. Guo W, Gao H, Li H, Ge S, Zhang F, Wang L, et al. Self-Assembly of a Multifunction DNA Tetrahedron for Effective Delivery of Aptamer PL1 and Pcsk9 siRNA Potentiate Immune Checkpoint Therapy for Colorectal Cancer. ACS Applied Materials & Interfaces. 2022;14(28):31634-44.

27. Yan J, Zhan X, Zhang Z, Chen K, Wang M, Sun Y, et al. Tetrahedral DNA nanostructures for effective treatment of cancer: advances and prospects. Journal of Nanobiotechnology. 2021;19(1):412.

28. Zhong L, Cai S, Huang Y, Yin L, Yang Y, Lu C, et al. DNA Octahedron-Based Fluorescence Nanoprobe for Dual Tumor-Related mRNAs Detection and Imaging. Analytical Chemistry. 2018;90(20):12059-66.

29. Hu G, He L, Iacovelli F, Falconi M. Intrinsic Dynamics Analysis of a DNA Octahedron by Elastic Network Model. Molecules. 2017;22(1):145.

30. Meng H-M, Zhang X, Lv Y, Zhao Z, Wang N-N, Fu T, et al. DNA Dendrimer: An Efficient Nanocarrier of Functional Nucleic Acids for Intracellular Molecular Sensing. ACS Nano. 2014;8(6):6171-81.

31. Zhang H, Ma Y, Xie Y, An Y, Huang Y, Zhu Z, et al. A Controllable Aptamer-Based Self-Assembled DNA Dendrimer for High Affinity Targeting, Bioimaging and Drug Delivery. Scientific Reports. 2015;5(1):10099.

32. Huang K, Ma H, Liu J, Huo S, Kumar A, Wei T, et al. Size-Dependent Localization and Penetration of Ultrasmall Gold Nanoparticles in Cancer Cells, Multicellular Spheroids, and Tumors in Vivo. ACS Nano. 2012;6(5):4483-93.

33. Zhu B, Zhao Y, Dai J, Wang J, Xing S, Guo L, et al. Preservation of DNA Nanostructure Carriers: Effects of Freeze–Thawing and Ionic Strength during Lyophilization and Storage. ACS Applied Materials & Interfaces. 2017;9(22):18434-9.

34. Amodio A, Adedeji AF, Castronovo M, Franco E, Ricci F. pH-Controlled Assembly of DNA Tiles. Journal of the American Chemical Society. 2016;138(39):12735-8.

35. Zhou W, Saran R, Liu J. Metal Sensing by DNA. Chemical Reviews. 2017;117(12):8272-325.

36. Nam K, Im BI, Kim T, Kim YM, Roh YH. Anisotropically Functionalized Aptamer-DNA Nanostructures for Enhanced Cell Proliferation and Target-Specific Adhesion in 3D Cell Cultures. Biomacromolecules. 2021;22(7):3138-47.

37. Yonezawa S, Koide H, Asai T. Recent advances in siRNA delivery mediated by lipid-based nanoparticles. Advanced Drug Delivery Reviews. 2020;154-155:64-78.

38. Yang C, Zhao H, Sun Y, Wang C, Geng X, Wang R, et al. Programmable manipulation of oligonucleotide–albumin interaction for elongated circulation time. Nucleic Acids Research. 2022;50(6):3083-95.

39. Ellington AD, Szostak JW. In vitro selection of RNA molecules that bind specific ligands. Nature. 1990;346(6287):818-22.

40. Tuerk C, Gold L. Systematic Evolution of Ligands by Exponential Enrichment: RNA Ligands to Bacteriophage T4 DNA Polymerase. Science. 1990;249(4968):505-10.

41. Tan W, Donovan MJ, Jiang J. Aptamers from Cell-Based Selection for Bioanalytical Applications. Chemical Reviews. 2013;113(4):2842-62.

42. Zhu H, Li J, Zhang X-B, Ye M, Tan W. Nucleic Acid Aptamer-Mediated Drug Delivery for Targeted Cancer Therapy. ChemMedChem. 2015;10(1):39-45.

43. Kong R, Chen Z, Ye M, Zhang X, Tan W. Cell-SELEX-based aptamer-conjugated nanomaterials for enhanced targeting of cancer cells. Science China Chemistry. 2011;54(8):1218-26.

44. Zhu G, Chen X. Aptamer-based targeted therapy. Advanced Drug Delivery Reviews. 2018;134:65-78.

45. Tewabe A, Abate A, Tamrie M, Seyfu A, Abdela Siraj E. Targeted Drug Delivery - From Magic Bullet to Nanomedicine: Principles, Challenges, and Future Perspectives. J Multidiscip Healthc. 2021;14:1711-24.

46. Ulbrich K, Holá K, Šubr V, Bakandritsos A, Tuček J, Zbořil R. Targeted Drug Delivery with Polymers and Magnetic Nanoparticles: Covalent and Noncovalent Approaches, Release Control, and Clinical Studies. Chemical Reviews. 2016;116(9):5338-431.

47. Li J, Wang Q, Xia G, Adilijiang N, Li Y, Hou Z, et al. Recent Advances in Targeted Drug Delivery Strategy for Enhancing Oncotherapy. Pharmaceutics. 2023;15(9):2233.

48. Gao F, Yin J, Chen Y, Guo C, Hu H, Su J. Recent advances in aptamer-based targeted drug delivery systems for cancer therapy. Frontiers in Bioengineering and Biotechnology. 2022;10.

49. Xie S, Sun W, Fu T, Liu X, Chen P, Qiu L, et al. Aptamer-Based Targeted Delivery of Functional Nucleic Acids. Journal of the American Chemical Society. 2023;145(14):7677-91.

50. Marverti G, Marraccini C, Martello A, D'Arca D, Pacifico S, Guerrini R, et al. Folic Acid–Peptide Conjugates Combine Selective Cancer Cell Internalization with Thymidylate Synthase Dimer Interface Targeting. Journal of Medicinal Chemistry. 2021;64(6):3204-21.

51. Reddy JA, Nelson M, Dircksen C, Vetzel M, Johnson T, Cross V, et al. Pre-clinical studies of EC2629, a highly potent folate- receptor-targeted DNA crosslinking agent. Scientific Reports. 2020;10(1):12772.

52. Chanphai P, Tajmir-Riahi HA. DNA binding efficacy with functionalized folic acid-PAMAM nanoparticles. Chemico-Biological Interactions. 2018;290:52-6.

53. Seeman NC. DNA in a material world. Nature. 2003;421(6921):427-31.

54. Zhan Y, Ma W, Zhang Y, Mao C, Shao X, Xie X, et al. DNA-Based Nanomedicine with Targeting and Enhancement of Therapeutic Efficacy of Breast Cancer Cells. ACS Applied Materials & Interfaces. 2019;11(17):15354-65.

55. Zhu G, Zheng J, Song E, Donovan M, Zhang K, Liu C, et al. Self-assembled, aptamer-tethered DNA nanotrains for targeted transport of molecular drugs in cancer theranostics. Proceedings of the National Academy of Sciences. 2013;110(20):7998-8003.

56. Charoenphol P, Bermudez H. Aptamer-Targeted DNA Nanostructures for Therapeutic Delivery. Molecular Pharmaceutics. 2014;11(5):1721-5.

57. Zhang X-Q, Xu X, Lam R, Giljohann D, Ho D, Mirkin CA. Strategy for Increasing Drug Solubility and Efficacy through Covalent Attachment to Polyvalent DNA–Nanoparticle Conjugates. ACS Nano. 2011;5(9):6962-70.

58. Strekowski L, Wilson B. Noncovalent interactions with DNA: An overview. Mutation Research/Fundamental and Molecular Mechanisms of Mutagenesis. 2007;623(1):3-13.

59. Powell Gray B, Kelly L, Ahrens DP, Barry AP, Kratschmer C, Levy M, et al. Tunable cytotoxic aptamer–drug conjugates for the treatment of prostate cancer. Proceedings of the National Academy of Sciences. 2018;115(18):4761-6.

60. Yoon S, Huang K-W, Reebye V, Spalding D, Przytycka TM, Wang Y, et al. Aptamer-Drug Conjugates of Active Metabolites of Nucleoside Analogs and Cytotoxic Agents Inhibit Pancreatic Tumor Cell Growth. Molecular Therapy - Nucleic Acids. 2017;6:80-8.

61. Pan Q, Nie C, Hu Y, Yi J, Liu C, Zhang J, et al. Aptamer-Functionalized DNA Origami for Targeted Codelivery of Antisense Oligonucleotides and Doxorubicin to Enhance Therapy in Drug-Resistant Cancer Cells. ACS Applied Materials & Interfaces. 2020;12(1):400-9.

62. Jiang Y, Pan X, Chang J, Niu W, Hou W, Kuai H, et al. Supramolecularly Engineered Circular Bivalent Aptamer for Enhanced Functional Protein Delivery. Journal of the American Chemical Society. 2018;140(22):6780-4.

63. Zamecnik PC, Stephenson ML. Inhibition of Rous sarcoma virus replication and cell transformation by a specific oligodeoxynucleotide. Proceedings of the National Academy of Sciences. 1978;75(1):280-4.

64. Shigdar S, Ward AC, De A, Yang CJ, Wei M, Duan W. Clinical applications of aptamers and nucleic acid therapeutics in haematological malignancies. British Journal of Haematology. 2011;155(1):3-13.

65. Hong S, Sun N, Liu M, Wang J, Pei R. Building a chimera of aptamer–antisense oligonucleotide for silencing galectin-1 gene. RSC Advances. 2016;6(113):112445-50.

66. Tanaka K, Okuda T, Kasahara Y, Obika S. Base-modified aptamers obtained by cell-internalization SELEX facilitate cellular uptake of an antisense oligonucleotide. Molecular Therapy - Nucleic Acids. 2021;23:440-9.

67. Zhu L, Bi J, Zheng L, Zhao Q, Shu X, Guo G, et al. In vitro inhibition of porcine reproductive and respiratory syndrome virus replication by short antisense oligonucleotides with locked nucleic acid modification. BMC Veterinary Research. 2018;14(1):109.

68. Fire A, Xu S, Montgomery MK, Kostas SA, Driver SE, Mello CC. Potent and specific genetic interference by double-stranded RNA in Caenorhabditis elegans. Nature. 1998;391(6669):806-11.

69. Pecot CV, Calin GA, Coleman RL, Lopez-Berestein G, Sood AK. RNA interference in the clinic: challenges and future directions. Nature Reviews Cancer. 2011;11(1):59-67.

70. Jeong JH, Mok H, Oh Y-K, Park TG. siRNA Conjugate Delivery Systems. Bioconjugate Chemistry. 2009;20(1):5-14.

71. Chu TC, Twu KY, Ellington AD, Levy M. Aptamer mediated siRNA delivery. Nucleic Acids Research. 2006;34(10):e73-e.

72. McNamara JO, Andrechek ER, Wang Y, Viles KD, Rempel RE, Gilboa E, et al. Cell type–specific delivery of siRNAs with aptamer-siRNA chimeras. Nature Biotechnology. 2006;24(8):1005-15.

73. Dassie JP, Liu X-y, Thomas GS, Whitaker RM, Thiel KW, Stockdale KR, et al. Systemic administration of optimized aptamer-siRNA chimeras promotes regression of PSMA-expressing tumors. Nature Biotechnology. 2009;27(9):839-46.

74. Wullner U, Neef I, Eller A, Kleines M, Tur KM, Barth S. Cell-Specific Induction of Apoptosis by Rationally Designed Bivalent Aptamer-siRNA Transcripts Silencing Eukaryotic Elongation Factor 2. Current Cancer Drug Targets. 2008;8(7):554-65.

75. Chong CR, Jänne PA. The quest to overcome resistance to EGFR-targeted therapies in cancer. Nature Medicine. 2013;19(11):1389-400.

76. Yu X, Ghamande S, Liu H, Xue L, Zhao S, Tan W, et al. Targeting EGFR/HER2/HER3 with a Three-in-One Aptamer-siRNA Chimera Confers Superior Activity against HER2⁺ Breast Cancer. Molecular Therapy - Nucleic Acids. 2018;10:317-30.

77. Lai W-Y, Wang W-Y, Chang Y-C, Chang C-J, Yang P-C, Peck K. Synergistic inhibition of lung cancer cell invasion, tumor growth and angiogenesis using aptamer-siRNA chimeras. Biomaterials. 2014;35(9):2905-14.

78. Rodriguez A, Griffiths-Jones S, Ashurst JL, Bradley A. Identification of Mammalian microRNA Host Genes and Transcription Units. Genome Research. 2004;14(10a):1902-10.

79. Horvitz HR, Sulston JE. Isolation and genetic characterization of cell-lineage mutants of the nematode Caenorhabditis elegans. Genetics. 1980;96(2):435-54.

80. Lin S, Gregory RI. MicroRNA biogenesis pathways in cancer. Nature Reviews Cancer. 2015;15(6):321-33.

81. Li Y, Kowdley KV. MicroRNAs in common human diseases. Genomics Proteomics Bioinformatics. 2012;10(5):246-53.

82. Dwivedi S, Purohit P, Sharma P. MicroRNAs and Diseases: Promising Biomarkers for Diagnosis and Therapeutics. Indian Journal of Clinical Biochemistry. 2019;34(3):243-5.

83. Hayes J, Peruzzi PP, Lawler S. MicroRNAs in cancer: biomarkers, functions and therapy. Trends in Molecular Medicine. 2014;20(8):460-9.

84. Dowdy SF. Overcoming cellular barriers for RNA therapeutics. Nat Biotechnol. 2017;35(3):222-9.

85. Esposito CL, Cerchia L, Catuogno S, De Vita G, Dassie JP, Santamaria G, et al. Multifunctional Aptamer-miRNA Conjugates for Targeted Cancer Therapy. Molecular Therapy. 2014;22(6):1151-63.

86. Wu X, Ding B, Gao J, Wang H, Fan W, Wang X, et al. Second-generation aptamer-conjugated PSMA-targeted delivery system for prostate cancer therapy. Int J Nanomedicine. 2011;6:1747-56.

87. The PONEE. Retraction: Differential SELEX in Human Glioma Cell Lines. PLOS ONE. 2020;15(2):e0228838.

88. Russo V, Paciocco A, Affinito A, Roscigno G, Fiore D, Palma F, et al. Aptamer-miR-34c Conjugate Affects Cell Proliferation of Non-Small-Cell Lung Cancer Cells. Mol Ther Nucleic Acids. 2018;13:334-46.

89. Iaboni M, Russo V, Fontanella R, Roscigno G, Fiore D, Donnarumma E, et al. Aptamer-miRNA-212 Conjugate Sensitizes NSCLC Cells to TRAIL. Molecular Therapy - Nucleic Acids. 2016;5.

90. Zanca C, Garofalo M, Quintavalle C, Romano G, Acunzo M, Ragno P, et al. PED is overexpressed and mediates TRAIL resistance in human non-small cell lung cancer. J Cell Mol Med. 2008;12(6a):2416-26.

91. Incoronato M, Garofalo M, Urso L, Romano G, Quintavalle C, Zanca C, et al. miR-212 increases tumor necrosis factor-related apoptosis-inducing ligand sensitivity in non-small cell lung cancer by targeting the antiapoptotic protein PED. Cancer Res. 2010;70(9):3638-46.

92. Miyoshi J, Toden S, Yoshida K, Toiyama Y, Alberts SR, Kusunoki M, et al. MiR-139-5p as a novel serum biomarker for recurrence and metastasis in colorectal cancer. Sci Rep. 2017;7:43393.

93. Zhao Y, Xu J, Le VM, Gong Q, Li S, Gao F, et al. EpCAM Aptamer-Functionalized Cationic Liposome-Based Nanoparticles Loaded with miR-139-5p for Targeted Therapy in Colorectal Cancer. Mol Pharm. 2019;16(11):4696-710.

94. Daei P, Ramezanpour M, Khanaki K, Tabarzad M, Nikokar I, Hedayati Ch M, et al. Aptamer-based Targeted Delivery of miRNA let-7d to Gastric Cancer Cells as a Novel Anti-Tumor Therapeutic Agent. Iran J Pharm Res. 2018;17(4):1537-49.

95. Carvalho J, Paiva A, Cabral Campello MP, Paulo A, Mergny J-L, Salgado GF, et al. Aptamer-based Targeted Delivery of a G-quadruplex Ligand in Cervical Cancer Cells. Scientific Reports. 2019;9(1):7945.

96. Taghdisi SM, Danesh NM, Ramezani M, Yazdian-Robati R, Abnous K. A Novel AS1411 Aptamer-Based Three-Way Junction Pocket DNA Nanostructure Loaded with Doxorubicin for Targeting Cancer Cells in Vitro and in Vivo. Molecular Pharmaceutics. 2018;15(5):1972-8.

97. Vindigni G, Raniolo S, Iacovelli F, Unida V, Stolfi C, Desideri A, et al. AS1411 Aptamer Linked to DNA Nanostructures Diverts Its Traffic Inside Cancer Cells and Improves Its Therapeutic Efficacy. Pharmaceutics. 2021;13(10):1671.

98. Norton JC, Piatyszek MA, Wright WE, Shay JW, Corey DR. Inhibition of human telomerase activity by peptide nucleic acids. Nature Biotechnology. 1996;14(5):615-9.

99. Arcamone F, Cassinelli G, Fantini G, Grein A, Orezzi P, Pol C, et al. Adriamycin, 14-hydroxydaimomycin, a new antitumor antibiotic from S. Peucetius var. caesius. Biotechnology and Bioengineering. 1969;11(6):1101-10.

100. Cortazar P, Justice R, Johnson J, Sridhara R, Keegan P, Pazdur R. US Food and Drug Administration approval overview in metastatic breast cancer. J Clin Oncol. 2012;30(14):1705-11.

101. Marinello J, Delcuratolo M, Capranico G. Anthracyclines as Topoisomerase II Poisons: From Early Studies to New Perspectives. Int J Mol Sci. 2018;19(11).

102. Zhang R, Zhu J, Sun D, Li J, Yao L, Meng S, et al. The Mechanism of Dynamic Interaction between Doxorubicin and Calf Thymus DNA at the Single-Molecule Level Based on Confocal Raman Spectroscopy. Micromachines (Basel). 2022;13(6).

103. Mejia G, Su L, Pandey P, Jeanne Dit Fouque K, McGoron AJ, Fernandez-Lima F, et al. Anticancer Drug Doxorubicin Spontaneously Reacts with GTP and dGTP. Chemical Research in Toxicology. 2023;36(4):660-8.

104. Kankeu C, Clarke K, Passante E, Huber HJ. Doxorubicin-induced chronic dilated cardiomyopathy—the apoptosis hypothesis revisited. Journal of Molecular Medicine. 2017;95(3):239-48.

105. Rotkrua P, Lohlamoh W, Watcharapo P, Soontornworajit B. A molecular hybrid comprising AS1411 and PDGF-BB aptamer, cholesterol, and doxorubicin for inhibiting proliferation of SW480 cells. Journal of Molecular Recognition. 2021;34(11):e2926.

106. Li W, Chen H, Yu M, Fang J. Targeted Delivery of Doxorubicin Using a Colorectal Cancer-Specific ssDNA Aptamer. The Anatomical Record. 2014;297(12):2280-8.

107. Bavi R, Hang Z, Banerjee P, Aquib M, Jadhao M, Rane N, et al. Doxorubicin-Conjugated Innovative 16-mer DNA Aptamer-Based Annexin A1 Targeted Anti-Cancer Drug Delivery. Mol Ther Nucleic Acids. 2020;21:1074-86.

108. Singh Y, Palombo M, Sinko PJ. Recent trends in targeted anticancer prodrug and conjugate design. Curr Med Chem. 2008;15(18):1802-26.

109. Paul F, Dörr J, Würfel J, Vogel HP, Zipp F. Early mitoxantrone-induced cardiotoxicity in secondary progressive multiple sclerosis. J Neurol Neurosurg Psychiatry. 2007;78(2):198-200.

110. Burns CP, Haugstad BN, North JA. Membrane transport of mitoxantrone by L1210 leukemia cells. Biochem Pharmacol. 1987;36(6):857-60.

111. Guan Y, Jiang S, Ye W, Ren X, Wang X, Zhang Y, et al. Combined treatment of mitoxantrone sensitizes breast cancer cells to rapalogs through blocking eEF-2K-mediated activation of Akt and autophagy. Cell Death & Disease. 2020;11(11):948.

112. Kingwell E, Koch M, Leung B, Isserow S, Geddes J, Rieckmann P, et al. Cardiotoxicity and other adverse events associated with mitoxantrone treatment for MS. Neurology. 2010;74(22):1822-6.

113. Ghalie RG, Edan G, Laurent M, Mauch E, Eisenman S, Hartung HP, et al. Cardiac adverse effects associated with mitoxantrone (Novantrone) therapy in patients with MS. Neurology. 2002;59(6):909-13.

114. Johari-Ahar M, Abdian M, Maleki S, Abbasgolizadeh P, Fathi F. Intercalation of anticancer drug mitoxantrone into DNA: Studied by spectral and surface plasmon resonance methods. Journal of Molecular Structure. 2023;1274:134509.

115. Barar J, Kafil V, Majd MH, Barzegari A, Khani S, Johari-Ahar M, et al. Multifunctional mitoxantrone-conjugated magnetic nanosystem for targeted therapy of folate receptor-overexpressing malignant cells. Journal of Nanobiotechnology. 2015;13(1):26.

116. Morrow CS, Peklak-Scott C, Bishwokarma B, Kute TE, Smitherman PK, Townsend AJ. Multidrug Resistance Protein 1 (MRP1, ABCC1) Mediates Resistance to Mitoxantrone via Glutathione-Dependent Drug Efflux. Molecular Pharmacology. 2006;69(4):1499-505.

117. Ling G, Zhang T, Zhang P, Sun J, He Z. Synergistic and complete reversal of the multidrug resistance of mitoxantrone hydrochloride by three-in-one multifunctional lipid-sodium glycocholate nanocarriers based on simultaneous BCRP and Bcl-2 inhibition. Int J Nanomedicine. 2016;11:4077-91.

118. Fox EJ. Mechanism of action of mitoxantrone. Neurology. 2004;63(12 Suppl 6):S15-8.

119. Rossi R, Montecucco A, Ciarrocchi G, Biamonti G. Functional characterization of the T4 DNA ligase: a new insight into the mechanism of action. Nucleic Acids Res. 1997;25(11):2106-13.

120. Lund AH, Duch M, Skou Pedersen F. Increased Cloning Efficiency by Temperature-Cycle Ligation. Nucleic Acids Research. 1996;24(4):800-1.

121. Zhang X, Wang Y, Zhou X. Ligation-Based qPCR-Amplification Assay for Radiolabel-Free Detection of ATP and NAD(+) with High Selectivity and Sensitivity. Anal Chem. 2019;91(2):1665-70.

122. Wang J, Liu F, Su T, Chang Y, Guo Q, Wang Q, et al. The phage T4 DNA ligase in vivo improves the survival-coupled bacterial mutagenesis. Microbial Cell Factories. 2019;18(1):107.

123. Bell DH. Characterization of the fluorescence of the antitumor agent, mitoxantrone. Biochimica et Biophysica Acta (BBA) - Gene Structure and Expression. 1988;949(1):132-7.

124. Jiramitmongkon K, Rotkrua P, Khanchaitit P, Arunpanichlert J, Soontornworajit B. Multifunctional molecular hybrid for targeted colorectal cancer cells: Integrating doxorubicin, AS1411 aptamer, and T9/U4 ASO. PLOS ONE. 2025;20(2):e0317559.

125. Dean P, Kenny B. Cell-surface nucleolin is sequestered into EPEC microcolonies and may play a role during infection. Microbiology (Reading). 2011;157(Pt 6):1761-7.

126. Dean P, Scott JA, Knox AA, Quitard S, Watkins NJ, Kenny B. The enteropathogenic E. coli effector EspF targets and disrupts the nucleolus by a process regulated by mitochondrial dysfunction. PLoS Pathog. 2010;6(6):e1000961.

127. Bie L, Wang Y, Jiang F, Xiao Z, Zhang L, Wang J. Insights into the binding mode of AS1411 aptamer to nucleolin. Frontiers in Molecular Biosciences. 2022;9.

128. Van den Avont A, Sharma-Walia N. Anti-nucleolin aptamer AS1411: an advancing therapeutic. Frontiers in Molecular Biosciences. 2023;10.

129. Iturriaga-Goyon E, Vivanco-Rojas O, Magaña-Guerrero FS, Buentello-Volante B, Castro-Salas I, Aguayo-Flores JE, et al. AS1411 Nucleolin-Specific Binding Aptamers Reduce Pathological Angiogenesis through Inhibition of Nucleolin Phosphorylation. Int J Mol Sci. 2021;22(23).

130. Dam DHM, Culver KSB, Odom TW. Grafting Aptamers onto Gold Nanostars Increases in Vitro Efficacy in a Wide Range of Cancer Cell Types. Molecular Pharmaceutics. 2014;11(2):580-7.

131. Florêncio e Silva E, Machado ES, Vasconcelos IB, Junior SA, L. Dutra JD, Freire RO, et al. Are the Absorption Spectra of Doxorubicin Properly Described by Considering Different Tautomers? Journal of Chemical Information and Modeling. 2020;60(2):513-21.

132. Gong C, Yang H, Wang S, Liu J, Li Z, Hu Y, et al. hTERT Promotes CRC Proliferation and Migration by Recruiting YBX1 to Increase NRF2 Expression. Frontiers in Cell and Developmental Biology. 2021;9.

133. Chen P, Gu WL, Gong MZ, Wang J, Li DQ. shRNA-mediated silencing of hTERT suppresses proliferation and promotes apoptosis in osteosarcoma cells. Cancer Gene Ther. 2017;24(8):325-32.

134. Zhao T, Hu F, Liu X, Tao Q. Blockade of telomerase reverse transcriptase enhances chemosensitivity in head and neck cancers through inhibition of AKT/ERK signaling pathways. Oncotarget. 2015;6(34):35908-21.

135. Jackson SR, Zhu C-H, Paulson V, Watkins L, Dikmen ZG, Gryaznov SM, et al. Antiadhesive Effects of GRN163L—An Oligonucleotide N3′→P5′ Thio-Phosphoramidate Targeting Telomerase. Cancer Research. 2007;67(3):1121-9.

136. Ozawa T, Gryaznov SM, Hu LJ, Pongracz K, Santos RA, Bollen AW, et al. Antitumor effects of specific telomerase inhibitor GRN163 in human glioblastoma xenografts. Neuro-Oncology. 2004;6(3):218-26.

137. Palumbo SL, Ebbinghaus SW, Hurley LH. Formation of a Unique End-to-End Stacked Pair of G-Quadruplexes in the hTERT Core Promoter with Implications for Inhibition of Telomerase by G-Quadruplex-Interactive Ligands. Journal of the American Chemical Society. 2009;131(31):10878-91.

138. Zhu X, Kumar R, Mandal M, Sharma N, Sharma HW, Dhingra U, et al. Cell cycle-dependent modulation of telomerase activity in tumor cells. Proceedings of the National Academy of Sciences. 1996;93(12):6091-5.

139. Holt SE, Aisner DL, Shay JW, Wright WE. Lack of cell cycle regulation of telomerase activity in human cells. Proceedings of the National Academy of Sciences. 1997;94(20):10687-92.

140. Qin Y, Tang B, Hu C-J, Xiao Y-F, Xie R, Yong X, et al. An hTERT/ZEB1 complex directly regulates E-cadherin to promote epithelial-to-mesenchymal transition (EMT) in colorectal cancer. Oncotarget. 2015;7(1).

141. Liu Z, Li Q, Li K, Chen L, Li W, Hou M, et al. Telomerase reverse transcriptase promotes epithelial-mesenchymal transition and stem cell-like traits in cancer cells. Oncogene. 2013;32(36):4203-13.

142. Usman S, Waseem NH, Nguyen TKN, Mohsin S, Jamal A, Teh MT, et al. Vimentin Is at the Heart of Epithelial Mesenchymal Transition (EMT) Mediated Metastasis. Cancers (Basel). 2021;13(19).

143. Venkova LS, Zerkalenkova EA, Minin AA. Vimentin Protects Cells Against Doxorubicin and Vincristine. Biochemistry (Moscow), Supplement Series A: Membrane and Cell Biology. 2018;12(3):255-60.

144. Cho Y, Lee YB, Lee J-H, Lee DH, Cho EJ, Yu SJ, et al. Modified AS1411 Aptamer Suppresses Hepatocellular Carcinoma by Up-Regulating Galectin-14. PLOS ONE. 2016;11(8):e0160822.

145. An J, Li P, Li J, Dietz R, Donath S. ARC is a critical cardiomyocyte survival switch in doxorubicin cardiotoxicity. Journal of Molecular Medicine. 2009;87(4):401-10.

146. Soundararajan S, Chen W, Spicer EK, Courtenay-Luck N, Fernandes DJ. The Nucleolin Targeting Aptamer AS1411 Destabilizes Bcl-2 Messenger RNA in Human Breast Cancer Cells. Cancer Research. 2008;68(7):2358-65.

147. Wang Q, Zhang L, Yuan X, Ou Y, Zhu X, Cheng Z, et al. The Relationship between the Bcl-2/Bax Proteins and the Mitochondria-Mediated Apoptosis Pathway in the Differentiation of Adipose-Derived Stromal Cells into Neurons. PLoS One. 2016;11(10):e0163327.

148. Sharifi S, Barar J, Hejazi MS, Samadi N. Doxorubicin Changes Bax /Bcl-xL Ratio, Caspase-8 and 9 in Breast Cancer Cells. Adv Pharm Bull. 2015;5(3):351-9.

149. Pilco-Ferreto N, Calaf GM. Influence of doxorubicin on apoptosis and oxidative stress in breast cancer cell lines. Int J Oncol. 2016;49(2):753-62.

150. Ma H, Zhang X, Pang L, Yu B, Cong H, Shen Y. Mn-dox metal-organic nanoparticles for cancer therapy and magnetic resonance imaging. Dyes and Pigments. 2022;199:110080.

151. Xu Y, Huang S-w, Ma Y-q, Ding H-m. Loading of DOX into a tetrahedral DNA nanostructure: the corner does matter. Nanoscale Advances. 2022;4(3):754-60.

152. Duo Y, Li Y, Chen C, Liu B, Wang X, Zeng X, et al. DOX-loaded pH-sensitive mesoporous silica nanoparticles coated with PDA and PEG induce pro-death autophagy in breast cancer. RSC Advances. 2017;7(63):39641-50.

153. Cheng Y, Zhao G, Zhang S, Nigim F, Zhou G, Yu Z, et al. AS1411-Induced Growth Inhibition of Glioma Cells by Up-Regulation of p53 and Down-Regulation of Bcl-2 and Akt1 via Nucleolin. PLoS One. 2016;11(12):e0167094.

154. Asai A, Oshima Y, Yamamoto Y, Uochi T-a, Kusaka H, Akinaga S, et al. A Novel Telomerase Template Antagonist (GRN163) as a Potential Anticancer Agent1. Cancer Research. 2003;63(14):3931-9.

155. Djojosubroto MW, Chin AC, Go N, Schaetzlein S, Manns MP, Gryaznov S, et al. Telomerase antagonists GRN163 and GRN163L inhibit tumor growth and increase chemosensitivity of human hepatoma. Hepatology. 2005;42(5):1127-36.

156. Lohlamoh W, Soontornworajit B, Rotkrua P. Anti-Proliferative Effect of Doxorubicin-Loaded AS1411 Aptamer on Colorectal Cancer Cell. Asian Pac J Cancer Prev. 2021;22(7):2209-219.

157. Semba S, Mizuuchi E, Yokozaki H. Requirement of phosphatase of regenerating liver-3 for the nucleolar localization of nucleolin during the progression of colorectal carcinoma. Cancer Science. 2010;101(10):2254-61.

158. Posner LE, Dukart G, Goldberg J, Bernstein T, Cartwright K. Mitoxantrone: an overview of safety and toxicity. Investigational New Drugs. 1985;3(2):123-32.

159. Sharma VR, Thomas SD, Miller DM, Rezzoug F. Nucleolin Overexpression Confers Increased Sensitivity to the Anti-Nucleolin Aptamer, AS1411. Cancer Investigation. 2018;36(9-10):475-91.

160. Hashemi M, Haghgoo Z, Yazdian-Robati R, Shahgordi S, Salmasi Z, Abnous K. Improved anticancer efficiency of Mitoxantrone by Curcumin loaded PLGA nanoparticles targeted with AS1411 aptamer. Nanomedicine Journal. 2021;8(1):21-9.

161. Vara JÁF, Casado E, de Castro J, Cejas P, Belda-Iniesta C, González-Barón M. PI3K/Akt signalling pathway and cancer. Cancer Treatment Reviews. 2004;30(2):193-204.

162. Misao J, Hayakawa Y, Ohno M, Kato S, Fujiwara T, Fujiwara H. Expression of bcl-2 Protein, an Inhibitor of Apoptosis, and Bax, an Accelerator of Apoptosis, in Ventricular Myocytes of Human Hearts With Myocardial Infarction. Circulation. 1996;94(7):1506-12.

APPENDICES

APPENDIX A

License and Copyright Policy of PLOS journal

Reuse of PLOS Article Content

Content Owned by Someone Else

Using Article Content Previously Published in Another Journal

Maps

Removal of Content Used Without Clear Rights

Trademarks and Symbols

Giving Proper Attribution for Use of Content

Licenses and Copyright

The following policy applies to all PLOS journals, unless otherwise noted.

Reuse of PLOS Article Content

PLOS applies the Creative Commons Attribution 4.0 International (CC BY) license, or other comparable licenses that allow free and unrestricted use, to articles and other works we publish. If you submit your paper for publication by PLOS, you retain copyright to your work and you agree to have the CC BY license applied to your work. If your institution or funder requires your work or materials to be published under a different license or dedicated to the public domain - for example Creative Commons 1.0 Universal (CC0) or Open Governmental License - this is permitted where the terms are equivalent to or more permissive than CC BY. PLOS requires that you as the author agree that anyone can reuse your article content in whole or part for any purpose, for free, even for commercial purposes. These permitted uses include but are not limited to self-archiving by authors of submitted, accepted and published versions of their papers in institutional repositories. Anyone may copy, redistribute, reuse, or modify the content as long as the author and original source are properly cited. This facilitates freedom in reuse and also ensures that

PLOS conten can be mined without barriers for the needs of research.

Content Owned by Someone Else

If your manuscript contains content such as photos, images, clipart, tables, audio files, videos, proprietary protocols, code, etc., that you or your co-authors do not own or did not create, we will require you to provide us with proof that either:

a. the material is in the public domain or available under an open access license compatible with CC BY 4.0, or
b. the owner of that content has given you written permission to use and publish the content under an open access CC BY 4.0 license.

Please note that purchasing copyright use is unlikely to meet this requirement, as many journals and publishers restrict the terms of purchased copyright use in ways that do not accommodate open access publication. In addition, we cannot accept Creative Commons licensed materials with additional non- commercial (CC BY-NC), share-alike (CC BY-SA), or non-derivative (CC BY-ND) clauses.

This Content Copyright Permission form can be used to request permissions from the relevant copyright holder, office, or representative. Authors should fill out the first page of the form with details on the material they wish to reuse and ask the copyright holder to complete and sign the second page of the form.

- If you do not have owner permission, we will ask you to remove the content and/or replace it with other content that you own or have such permission to use.

Don't assume that you can use any content you find on the Internet, or that the content is fair game just because it isn't clear who the owner is or what license applies. It's up to you to ascertain what rights you have—if any—to use that content.

Under no circumstances should your manuscript contain third party trade secret information.

Using Article Content Previously Published in Another Journal

Many authors assume that if they previously published a paper through another publisher, they own the rights to that content and they can freely use that content in

their PLOS paper, but that's not necessarily the case – it depends on the license that covers the other paper. Some publishers allow free and unrestricted re-use of article content they own, such as under the CC BY license. Other publishers use licenses that allow re-use only if the same license is applied by the person or publisher re-using the content.

If the paper was published under a CC BY license or another license that allows free and unrestricted use, you may use the content in your PLOS paper provided that you give proper attribution, as explained above

If the content was published under a more restrictive license, you must ascertain what rights you have under that license. At a minimum, review the license to make sure you can use the content. Contact that publisher if you have any questions about the license terms – PLOS staff cannot give you legal advice about your rights to use third-party content. If the license does not permit you to use the content in a paper that will be covered by an unrestricted license, you must obtain written permission from the publisher to use the content in your PLOS paper. Please do not include any content in your PLOS paper which you do not have rights to use, and always give proper attribution.

Maps

Any maps included or created as part of a figure must use a basemap tile, shapefile, or image compatible with our CC BY 4.0 license. The basemap refers to the foundational geographic layer of the map (possibly including country boundaries, for example) onto which other layers of data are plotted. Satellite and aerial images may also be used as basemaps.

If your submission file inventory includes a map, we will ask you to provide a direct link to the source of the basemap and provide attribution to this source in the corresponding figure legend. We will also ask you to provide information regarding the terms of use or license information for the map.

If you created the map in a software program like R or ArcGIS, please locate the source of the basemap within the package used to generate the map.

Several sources provide map data and shapefiles within the public domain or with open access licenses:

- U.S. Geological Survey (USGS) - (https://www.usgs.gov/)
- Natural Earth - (http://www.naturalearthdata.com/about/terms-of-use/)
- OpenStreetMap - (https://www.openstreetmap.org/copyright)
- CIA Factbook - (Maps - The World Factbook)

As with all content, we ask that authors respect map providers' requirements for attribution.

Removal of Content Used Without Clear Rights

PLOS reserves the right to remove any photos, captures, images, figures, tables, illustrations, audio and video files, or other confidential or proprietary content, from any article, whether before or after publication, if concerns are raised about copyright, license, or permissions and the authors are unable to provide documentation confirming that appropriate permissions were obtained for publication of the content in question under a CC BY 4.0 license.

Trademarks and Symbols

Please note that we cannot publish copyright symbols such as ©, ®, or ™. We are also unable to publish logos or other brand-related content.

Acceptable Licenses for Data Repositories

If any relevant accompanying data is submitted to repositories with stated licensing policies, the policies should not be more restrictive than CC BY 4.0.

Giving Proper Attribution for Use of Content

When citing a PLOS research article, use the "Vancouver style", as outlined in our Submission Guidelines. For example:

> Kaltenbach LS et al. (2007) Huntingtin Interacting Proteins Are Genetic Modifiers of Neurodegeneration. PLOS Genet 3(5): e82. doi:10.1371/journal.pgen.0030082.

When citing non-article content from a PLOS website (e.g., blog content), provide a link to the content, and cite the title and author(s) of that content.

APPENDIX B

Attribution 4.0 International

Deed

Canonical URL:
https://creativecommons.org/license/by/4.0

See the legal code

You are free to:

Share — copy and redistribute the material in any medium or format for any purpose, even commercially.

Adapt — remix, transform, and build upon the material for any purpose, even commercially.

The licensor cannot revoke these freedoms as long as you follow the license terms.

Under the following terms:

Attribution — You must give appropriate credit , provide a link to the license, and indicate if changes were made . You may do so in any reasonable manner, but not in any way that suggests the licensor endorses you or your use.

No additional restrictions — You may not apply legal terms or technological measures that legally restrict others from doing anything the license permits.

Notices:

You do not have to comply with the license for elements of the material in the public domain or where your use is permitted by an applicable exception or

limitation .

No warranties are given. The license may not give you all of the permissions necessary for your intended use. For example, other rights such as publicity, privacy, or moral rights may limit how you use the material.

Notice

This deed highlights only some of the key features and terms of the actual license. It is not a license and has no legal value. You should carefully review all of the terms and conditions of the actual license before using the licensed material.

Creative Commons is not a law firm and does not provide legal services. Distributing, displaying, or linking to this deed or the license that it summarizes does not create a lawyer-client or any other relationship.

Creative Commons is the nonprofit behind the open licenses and other legal tools that allow creators to share their work. Our legal tools are free to use.

- Learn more about our work
- Learn more about CC Licensing
- Support our work
- Use the license for your own material.
- Licenses List
- Public Domain List

Footnotes

appropriate credit — If supplied, you must provide the name of the creator and attribution parties, a copyright notice, a license notice, a disclaimer notice, and a link to the material. CC licenses prior to Version 4.0

also require you to provide the title of the material if supplied, and may have other slight differences.

- More info

indicate if changes were made — In 4.0, you must indicate if you modified the material and retain an indication of previous modifications. In 3.0 and earlier license versions, the indication of changes is only required if you create a derivative.

- Making guide
- More info

technological measures — The license prohibits application of effective technological measures, defined with reference to Article 11 of the WIPO Copyright Treaty.

- More info

exception or limitation — The rights of users under exceptions and limitations, such as fair use and fair dealing, are not affected by the CC licenses.

- More info

publicity, privacy, or moral rights — You may need to get additional permissions before using the material as you intend.

- More info

BIOGRAPHY

Name	Kanpitcha Jiramitmongkon
Educational Attainment	2002: Bachelor degree of Science (Chemistry) Rajabhat Institute Suan Dusit, Thailand 2006: Master degree of Science (Chemistry) King Mongkut's Institute of Technology Ladkrabang, Thailand
Scholarship (If any)	2022 - 2025: Full Scholarship for Research, Internationalization, and Education, Thammasat University

Publications

1. Jiramitmongkon, K.; Rotkrua, P.; Khanchaitit, P.; Arunpanichlert, J.; Soontornworajit, B. Multifunctional molecular hybrid for targeted colorectal cancer cells: Integrating doxorubicin, AS1411 aptamer, and T9/U4 ASO. *PLOS ONE* **2025**, *20* (2), e0317559. DOI: 10.1371/journal.pone.0317559

2. Pikulthong, W.; Aunkitkancharoen, P.; Chaothum, W.; Jorntrakan, N.; Jiramitmongkon, K.; Rotkrua, P.; Arunpanichlert, J.; Soontornworajit, B. Development of gelatin particles encapsulating PDGF-BB aptamer for the efficient drug delivery system. *J Adv Biotechnol Exp Ther.* **2025**, 8(2), 259-271.